PTEP

Prog. Theor. Exp. Phys. **2021**, 013D01 (27 pages)
DOI: 10.1093/ptep/ptaa163

Hartree–Fock–Bogoliubov theory for odd-mass nuclei with a time-odd constraint and application to deformed halo nuclei

Haruki Kasuya[1] and Kenichi Yoshida[2,*]

[1]*Yukawa Institute for Theoretical Physics, Kyoto University, Kyoto 606-8502, Japan*
[2]*Department of Physics, Kyoto University, Kyoto 606-8502, Japan*
*E-mail: kyoshida@ruby.scphys.kyoto-u.ac.jp

Received May 15, 2020; Revised November 9, 2020; Accepted November 10, 2020; Published November 13, 2020

We show that the lowest-energy solution of the Hartree–Fock–Bogoliubov (HFB) equation has even particle-number parity as long as the time-reversal symmetry is conserved in the HFB Hamiltonian without null eigenvalues. Based on this finding, we give a rigorous foundation for a method for solving the HFB equation to describe the ground state of odd-mass nuclei by employing a time-reversal antisymmetric constraint operator to the Hamiltonian, where one obtains directly the ground state as a self-consistent solution of the cranked-HFB-type equation. Numerical analysis is performed for the neutron-rich Mg isotopes with a reasonable choice for the operator, and it is demonstrated that the anomalous increase in the matter radius of ^{37}Mg is well described when the last neutron occupies a low-angular-momentum orbital in the framework of the nuclear energy density functional method, revealing the deformed halo structure.

Subject Index D10, D11, D12, D13

1. Introduction

Odd-mass nuclei, composed of an odd number of nucleons, display unique features that one cannot observe in even–even nuclei. Even–even nuclei, for instance, have spin $J^\pi = 0^+$ in the ground state, where nucleons are paired off due to the correlation, while odd-mass nuclei have nonzero ground-state spin, where the last nucleon does not take part in the pair correlation and is responsible for the total spin. The spin gives us information on the single-particle orbitals near the Fermi level. With the increase in structure information on unstable nuclei thanks to recent advancements in radioactive-isotope beam technology [1], more and more exotic features in odd-mass nuclei have been showing up. Highlights in the latest discoveries include the shape staggering in $^{181-185}$Hg [2], and the deformed halo structures of ^{31}Ne [3,4] and ^{37}Mg [5,6]. A great theoretical challenge under these circumstances is to describe odd-mass nuclei in a wide mass region of the nuclear chart, where the pair correlation, shape deformation, and weak binding of nucleons are all considered in a unified manner.

Nuclear density-functional theory (DFT) or the self-consistent mean-field model have been extensively employed for describing the systematic features of both ground and excited states [7,8]. The nuclear landscape has been investigated in the framework of both non-relativistic and relativistic energy-density functional (EDF) methods [9,10]. The Hartree–Fock–Bogoliubov (HFB) theory or the Kohn–Sham–Bogoliubov–de Gennes scheme in DFT is capable of providing a unified description of the ground-state properties for both even–even nuclei and odd-mass nuclei taking superfluidity and shape deformation into account [11]. In spite of the successful application of DFT, the calculations

have been mostly restricted to even–even nuclei, and odd-mass nuclei remain largely unexplored [12]. This may be partly because the primary interest has been on determining the drip lines [13]. With the recent advent of computational resources sufficient to perform global calculations in the framework of DFT, systematic odd–even alternations in atomic nuclei such as the odd–even staggering of the binding energies have attracted renewed interest [14].

There seem to be many obstacles to tackling the systematic investigation of odd-mass nuclei in DFT, some of which are:

(1) The coexistence of multiple levels at low energy: to excite even–even nuclei we have to break at least one pair of nucleons whose binding energy is of the order of 1–2 MeV, whereas for odd-mass nuclei an excitation can be achieved by putting up the last nucleon by a few hundred keV. As a result, one-quasiparticle and phonon states appear in the low-excitation energy and they can admix with one another [15], and thus the HFB describes the ground state of even–even nuclei better. High-precision calculation with high accuracy is also required for resolving the near degeneracy of several levels and identifying the ground state for odd-mass nuclei. This is not restricted to DFT but is a challenge for any theoretical model.
(2) Non-vanishing time-odd densities: an EDF is a time-even scalar constructed from various densities, and includes the densities and currents that are odd with respect to time reversal to preserve the Galilean or Lorentz invariance and to properly describe, e.g., the spin-dependent observables. While the time-odd densities and the related time-odd fields automatically vanish for the ground state of even–even nuclei, they are nonzero in odd-mass nuclei where the time-reversal symmetry is intrinsically broken [7]. Allowing the breaking of time-reversal symmetry increases the computational cost [16]. Furthermore, the EDFs commonly used in practical calculations are phenomenologically constructed by using the properties of time-even states only. Thus, in the non-relativistic case, the coupling constants of time-odd fields are highly uncertain. In the relativistic case, on the other hand, the coupling constants of time-odd fields are defined from those of time-even fields through the Lorentz invariance, so there are no such uncertainties [17–20].
(3) Complexity of the blocking procedure: one cannot usually obtain the ground state of odd-mass nuclei as the lowest-energy solution, so we need an additional procedure to excite one quasiparticle on top of the ground state of even–even nuclei [21]. Therefore, pragmatic techniques are needed in an actual calculation [22,23].

We are going to focus on (3).

In this study, we investigate the non-relativistic case and show that the Bogoliubov transformation, the particle-number parity, and the time-reversal symmetry in HFB are closely related to one another. From these findings, we can give a rigorous foundation for a method initiated by Bertsch et al. [24] to describe the ground state of an odd-particle system as the lowest-energy state under an appropriate time-odd constraint in HFB theory. This method has a high affinity with DFT in the sense that either an odd-particle system or an even-particle system is described as the ground state uniformly. We apply this method to the neutron-rich Mg isotopes near the drip line and demonstrate that it produces the exotic behavior in radii observed experimentally.

The article is organized as follows. In Sect. 2, after recapitulating the basics of HFB theory, the relationships among the Bogoliubov transformation, the particle-number parity, and the time-reversal symmetry are presented. In Sect. 3, based on the relationships found in Sect. 2, we give the foundation

for a method describing the ground-state of odd-mass nuclei under a time-odd constraint. In Sect. 4 we give a numerical procedure for describing weakly bound neutron-rich nuclei by employing the non-relativistic Skyrme-type EDF with the inclusion of the time-odd fields. Then, the results of the numerical analysis for Mg isotopes are presented. Finally, a summary is given in Sect. 5.

Part of the preliminary results of this work are reported in Ref. [25].

2. Hartree–Fock–Bogoliubov theory for even- and odd-particle systems

2.1. Basics of HFB theory

We begin by recalling the basics of HFB theory. The notation used here follows Ref. [11]. The Bogoliubov quasiparticle (qp) creation and annihilation operators $\hat{\beta}_k^\dagger, \hat{\beta}_k$ are defined as linear combinations of the single-particle (sp) creation and annihilation operators $\hat{c}_k^\dagger, \hat{c}_k$:

$$\hat{\beta}_k^\dagger = \sum_l (U_{lk}\hat{c}_l^\dagger + V_{lk}\hat{c}_l), \tag{1}$$

where the indices k and l run over the whole configuration space ($k = 1, \ldots, M$). Since we consider spin-1/2 particles, M is an even number. The Bogoliubov transformation between the qp and sp bases is represented by the $2M \times 2M$ matrix

$$\mathcal{W} \coloneqq \begin{pmatrix} U & V^* \\ V & U^* \end{pmatrix} \tag{2}$$

as

$$\begin{pmatrix} \hat{\beta} \\ \hat{\beta}^\dagger \end{pmatrix} = \mathcal{W}^\dagger \begin{pmatrix} \hat{c} \\ \hat{c}^\dagger \end{pmatrix}. \tag{3}$$

In order to satisfy the fermion anticommutation relations for quasiparticles, $\mathcal{W}$ must be unitary: $\mathcal{W}^\dagger\mathcal{W} = \mathcal{W}\mathcal{W}^\dagger = I_{2M}$, with I_n representing the $n \times n$ identity matrix. The ground state wave function of the many-body system in HFB theory, or the HFB vacuum, $|\Phi\rangle$, is defined as the vacuum of the quasiparticles:

$$\hat{\beta}_k |\Phi\rangle = 0 \qquad \text{for all } k. \tag{4}$$

The complete information about $|\Phi\rangle$ is contained by the density matrix $\rho_{kl} \coloneqq \langle\Phi|\hat{c}_l^\dagger\hat{c}_k|\Phi\rangle = (V^*V^\mathsf{T})_{kl}$ and pairing tensor $\kappa_{kl} \coloneqq \langle\Phi|\hat{c}_l\hat{c}_k|\Phi\rangle = (V^*U^\mathsf{T})_{kl}$, or by the generalized density matrix

$$\mathcal{R} \coloneqq \begin{pmatrix} \rho & \kappa \\ -\kappa^* & 1-\rho^* \end{pmatrix} = \mathcal{W} \begin{pmatrix} O_M & O_M \\ O_M & I_M \end{pmatrix} \mathcal{W}^\dagger, \tag{5}$$

where O_n represents the $n \times n$ zero matrix. The unitarity of $\mathcal{W}$ guarantees that $\mathcal{R}$ is idempotent: $\mathcal{R}^2 = \mathcal{R}$. Under the idempotency of $\mathcal{R}$, the variational principle with a constraint on the expectation value of the particle number, $\delta\langle\Phi|\hat{H} - \lambda\hat{N}|\Phi\rangle = 0$, where $\hat{H}$, $\hat{N}$, and λ are the Hamiltonian of the system, the particle-number operator, and the chemical potential, respectively, leads $\mathcal{R}$ to commute with the HFB Hamiltonian

$$\mathcal{H} \coloneqq \begin{pmatrix} h - \lambda I_M & \Delta \\ -\Delta^* & -h^* + \lambda I_M \end{pmatrix}, \tag{6}$$

where $h_{kl} \coloneqq \delta \langle\Phi|\hat{H}|\Phi\rangle / \delta\rho_{lk}$ and $\Delta_{kl} \coloneqq \delta \langle\Phi|\hat{H}|\Phi\rangle / \delta\kappa^*_{kl}$ are the sp and pair Hamiltonian, respectively. It follows that $\mathcal{R}$ and $\mathcal{H}$ are simultaneously diagonalized, and thus the HFB equations are represented in a matrix form as

$$\begin{pmatrix} h - \lambda I_M & \Delta \\ -\Delta^* & -h^* + \lambda I_M \end{pmatrix} \begin{pmatrix} U & V^* \\ V & U^* \end{pmatrix} = \begin{pmatrix} U & V^* \\ V & U^* \end{pmatrix} \begin{pmatrix} E & 0 \\ 0 & -E \end{pmatrix}, \tag{7}$$

or

$$\mathcal{W}^\dagger \mathcal{H} \mathcal{W} = \mathcal{E}, \tag{8}$$

where $\mathcal{E} \coloneqq \mathrm{diag}(E, -E)$ and E is a diagonal matrix of qp energies E_k. Note that the HFB Hamiltonian inherently has the particle–hole symmetry:

$$\Sigma_x \mathcal{H}^* \Sigma_x = -\mathcal{H}, \tag{9}$$

where

$$\Sigma_x \coloneqq \begin{pmatrix} 0 & 1 \\ 1 & 0 \end{pmatrix} \otimes I_M = \begin{pmatrix} O_M & I_M \\ I_M & O_M \end{pmatrix}.$$

It follows that when φ_k is an eigenvector of $\mathcal{H}$ with eigenvalue E_k, $\Sigma_x \varphi^*_k$ is also an eigenvector with eigenvalue $-E_k$. Thus, the eigenvalues of $\mathcal{H}$ always come in pairs of opposite sign, but the theory says nothing about the individual signs of E_k. Therefore, we have to choose for each k ($k = 1, \ldots, M$) whether to take E_k positive or negative. This choice for the solution of the HFB equations in superfluid systems corresponds to the choice of "occupied" or "unoccupied" orbits for the solution of the Hartree–Fock (HF) equations in normal systems. A naïve choice to describe the ground state of the system is to take all E_k positive, as in the HF case the ground state is obtained by filling sp levels from below. Indeed, the state obtained by this choice has the lowest energy in the sense that all the qp excitations cost positive energies. As will be seen below, however, the state is not always the ground state of the system with the desired particle-number parity [26]. We shall therefore call the state obtained by taking all E_k positive the lowest-energy state, as distinct from other choices, and the ground state with the proper particle-number parity.

2.2. Particle-number parity and the Bogoliubov transformation

We first show a relationship between the particle-number parity π_N and the Bogoliubov transformation matrix $\mathcal{W}$. The famous theorem of Bloch and Messiah says that a unitary matrix $\mathcal{W}$ of the form in Eq. (2) can always be decomposed into three matrices of very special form [27]:

$$\mathcal{W} = \begin{pmatrix} D & 0 \\ 0 & D^* \end{pmatrix} \begin{pmatrix} \bar{U} & \bar{V} \\ \bar{V} & \bar{U} \end{pmatrix} \begin{pmatrix} C & 0 \\ 0 & C^* \end{pmatrix}. \tag{10}$$

Here, C and D are unitary matrices, and $\bar{U}, \bar{V}$ are real matrices of the general form

$$\bar{U} = \begin{pmatrix} O_{N_1} & & & & \\ & \bar{U}^{(1)} & & 0 & \\ & & \bar{U}^{(2)} & & \\ & & & \ddots & \\ & 0 & & & \bar{U}^{(N_2)} \\ & & & & & I_{N_3} \end{pmatrix}, \quad \bar{V} = \begin{pmatrix} I_{N_1} & & & & \\ & \bar{V}^{(1)} & & 0 & \\ & & \bar{V}^{(1)} & & \\ & & & \ddots & \\ & 0 & & & \bar{V}^{(N_2)} \\ & & & & & O_{N_3} \end{pmatrix}, \tag{11}$$

where $N_3 = M - N_1 - 2N_2$, and $\bar{U}^{(p)}, \bar{V}^{(p)}$ are 2×2 matrices of the form

$$\bar{U}^{(p)} = \begin{pmatrix} u_p & 0 \\ 0 & u_p \end{pmatrix}, \quad \bar{V}^{(p)} = \begin{pmatrix} 0 & v_p \\ -v_p & 0 \end{pmatrix} \qquad (p = 1, 2, \ldots, N_2), \tag{12}$$

where u_p and v_p satisfy the conditions $u_p > 0$, $v_p > 0$, $u_p^2 + v_p^2 = 1$ $(p = 1, 2, \ldots, N_2)$. One can explicitly construct the HFB vacuum $|\Phi\rangle$ in terms of the so-called canonical basis defined as $\hat{a}_k^\dagger = \sum_l D_{lk} \hat{c}_l^\dagger$ [11]:

$$|\Phi\rangle = \prod_{i=1}^{N_1} \hat{a}_i^\dagger \prod_{p=1}^{N_2} (u_p + v_p \hat{a}_p^\dagger \hat{a}_{\bar{p}}^\dagger) \, |0\rangle. \tag{13}$$

Here, $|0\rangle$ is the empty state defined as $\hat{c}_k \, |0\rangle = 0$ for all k. The index $\bar{p}$ represents an orbital paired with the orbital p, and N_2 indicates the maximum number of pairs in $|\Phi\rangle$. N_1 represents the number of unpaired particles, and corresponds to the seniority number in the quasi-spin theory [28]. Depending on whether N_1 is even or odd, $|\Phi\rangle$ is a superposition of states with either even or odd particles, but never both. This means that the HFB vacuum $|\Phi\rangle$ is an eigenstate of the operator $\hat{P}_N = e^{i\pi \hat{N}}$, where $\hat{N}$ is the particle-number operator. The eigenvalue $\pi_N = (-1)^{N_1}$ is a good quantum number, called the particle-number parity, or the number parity for short [29]. Note that the number parity has nothing to do with the average particle number $\langle \Phi | \hat{N} | \Phi \rangle$, which can be even, odd, or fractional, depending on the value of the chemical potential λ in Eq. (6).

Taking the determinant of both sides of Eq. (10), we obtain

$$\begin{aligned} \det \mathcal{W} &= \det \begin{pmatrix} D & 0 \\ 0 & D^* \end{pmatrix} \det \begin{pmatrix} \bar{U} & \bar{V} \\ \bar{V} & \bar{U} \end{pmatrix} \det \begin{pmatrix} C & 0 \\ 0 & C^* \end{pmatrix} \\ &= |\det D|^2 \det(\bar{U} + \bar{V}) \det(\bar{U} - \bar{V}) \, |\det C|^2 \\ &= \det \left\{ \mathrm{diag} \left[I_{N_1}, \begin{pmatrix} u_1 & v_1 \\ -v_1 & u_1 \end{pmatrix}, \begin{pmatrix} u_2 & v_2 \\ -v_2 & u_2 \end{pmatrix}, \ldots, \begin{pmatrix} u_{N_2} & v_{N_2} \\ -v_{N_2} & u_{N_2} \end{pmatrix}, I_{N_3} \right] \right. \\ &\qquad \left. \times \mathrm{diag} \left[-I_{N_1}, \begin{pmatrix} u_1 & -v_1 \\ v_1 & u_1 \end{pmatrix}, \begin{pmatrix} u_2 & -v_2 \\ v_2 & u_2 \end{pmatrix}, \ldots, \begin{pmatrix} u_{N_2} & -v_{N_2} \\ v_{N_2} & u_{N_2} \end{pmatrix}, I_{N_3} \right] \right\} \\ &= \det \begin{pmatrix} -I_{N_1} & 0 \\ 0 & I_{M-N_1} \end{pmatrix} = (-1)^{N_1}, \end{aligned} \tag{14}$$

where we used the fact that C and D are unitary matrices, and

$$\begin{pmatrix} u_p & v_p \\ -v_p & u_p \end{pmatrix}\begin{pmatrix} u_p & -v_p \\ v_p & u_p \end{pmatrix} = \begin{pmatrix} u_p^2+v_p^2 & 0 \\ 0 & u_p^2+v_p^2 \end{pmatrix} = \begin{pmatrix} 1 & 0 \\ 0 & 1 \end{pmatrix} \qquad (p=1,2,\ldots,N_2).$$

Equation (14) shows that $\det\mathcal{W}$ is nothing less than the number parity:

$$\pi_N = \det\mathcal{W}. \tag{15}$$

Before continuing, we give a useful formula that relates the number parity π_N to the HFB Hamiltonian $\mathcal{H}$ and the qp energies E_k. The fact that the determinant of $\mathcal{W}$ is either $+1$ or -1 implies that $\mathcal{W}$ can be unitarily transformed into an orthogonal matrix. In fact, by use of the unitary matrix

$$\mathcal{X} = \frac{1}{\sqrt{2}}\begin{pmatrix} 1 & 1 \\ i & -i \end{pmatrix} \otimes I_M, \tag{16}$$

$\mathcal{W}$ is transformed into a real orthogonal matrix:

$$\mathcal{W}_\mathcal{X} \coloneqq \mathcal{X}\mathcal{W}\mathcal{X}^\dagger = \begin{pmatrix} \mathrm{Re}(U+V) & \mathrm{Im}(U+V) \\ -\mathrm{Im}(U-V) & \mathrm{Re}(U-V) \end{pmatrix}. \tag{17}$$

In the same way, the HFB Hamiltonian $\mathcal{H}$ is transformed into a pure-imaginary skew-symmetric matrix:

$$\mathcal{H}_\mathcal{X} \coloneqq \mathcal{X}\mathcal{H}\mathcal{X}^\dagger = i\begin{pmatrix} \mathrm{Im}(h'+\Delta) & -\mathrm{Re}(h'-\Delta) \\ \mathrm{Re}(h'+\Delta) & \mathrm{Im}(h'-\Delta) \end{pmatrix}, \tag{18}$$

where $h' \coloneqq h - \lambda I_M$. Then the HFB equations in Eq. (8) are rewritten as follows:

$$\mathcal{W}_\mathcal{X}^\mathsf{T}\mathcal{H}_\mathcal{X}\mathcal{W}_\mathcal{X} = \mathcal{E}_\mathcal{X}, \tag{19}$$

where

$$\mathcal{E}_\mathcal{X} \coloneqq \mathcal{X}\mathcal{E}\mathcal{X}^\dagger = -i\begin{pmatrix} 0 & E \\ -E & 0 \end{pmatrix}. \tag{20}$$

Since both sides of Eq. (19) are $2M \times 2M$ skew-symmetric matrices, we can take Pfaffian[1] of each side. Using the properties of the Pfaffian ($\mathrm{pf}(\mathcal{W}_{\mathcal{X}}^{\mathsf{T}}\mathcal{H}_{\mathcal{X}}\mathcal{W}_{\mathcal{X}}) = \det\mathcal{W}_{\mathcal{X}}\,\mathrm{pf}\,\mathcal{H}_{\mathcal{X}}$ and $\mathrm{pf}\,\mathcal{E}_{\mathcal{X}} = (-1)^{M(M-1)/2}\det(-iE)$) we obtain

$$\det\mathcal{W}_{\mathcal{X}}\,\mathrm{pf}\,\mathcal{H}_{\mathcal{X}} = (-1)^{M(M-1)/2}\det(-iE).$$

Since M is an even number, $E = \mathrm{diag}(E_1, E_2, \ldots, E_M)$, and $\det\mathcal{W}_{\mathcal{X}} = \det\mathcal{W}$, it follows that

$$\det\mathcal{W}\,\mathrm{pf}\,\mathcal{H}_{\mathcal{X}} = \prod_{k=1}^{M} E_k. \tag{21}$$

Thus, we arrive at a useful relation between the number parity π_N, the HFB Hamiltonian $\mathcal{H}$, and the qp energies E_k:

$$\pi_N\,\mathrm{pf}\,\mathcal{H}_{\mathcal{X}} = \prod_{k=1}^{M} E_k. \tag{22}$$

We emphasize that Eq. (22) is a general relation that holds regardless of the signs of E_k. For the lowest-energy state, the right-hand side of Eq. (22) is positive by definition. Therefore, the number parity of the lowest-energy state, π_N^{LE}, depends only on the sign of $\mathrm{pf}\,\mathcal{H}_{\mathcal{X}}$:

$$\pi_N^{\mathrm{LE}} = \mathrm{sgn}\,\mathrm{pf}\,\mathcal{H}_{\mathcal{X}}. \tag{23}$$

Note that an equivalent formula to Eq. (23) is obtained in Ref. [32] to investigate topological properties of a one-dimensional superfluid system.

2.3. *Symmetries in HFB theory*

Before investigating the time-reversal symmetry of the HFB Hamiltonian, we discuss a general property of the symmetry in HFB theory. Since the HFB equations are nonlinear, the HFB Hamiltonian $\mathcal{H}$ does not necessarily hold the same symmetries as the Hamiltonian of the system $\hat{H}$. Nevertheless, certain symmetries are still conserved in HFB theory. Such symmetries are called self-consistent symmetries, and they often significantly reduce the dimension of the eigenvalue problem [33].

[1] For a $2n \times 2n$ skew-symmetric matrix A with matrix elements a_{ij}, the Pfaffian of A is defined as

$$\mathrm{pf}(A) = \frac{1}{2^n n!}\sum_{\sigma\in S_{2n}}\mathrm{sgn}(\sigma)a_{\sigma(1)\sigma(2)}a_{\sigma(3)\sigma(4)}\cdots a_{\sigma(2n-1)\sigma(2n)},$$

where S_{2n} is the set of permutations on $2n$ elements. Pfaffians have the following properties:
For a $2n \times 2n$ skew-symmetric matrix A,

$$(\mathrm{pf}\,A)^2 = \det A.$$

For a $2n \times 2n$ skew-symmetric matrix A and an arbitrary $2n \times 2n$ matrix B,

$$\mathrm{pf}(B^{\mathsf{T}}AB) = \det B\,\mathrm{pf}\,A.$$

For an arbitrary $n \times n$ matrix C,

$$\mathrm{pf}\begin{pmatrix} 0 & C \\ -C^{\mathsf{T}} & 0 \end{pmatrix} = (-1)^{n(n-1)/2}\det C.$$

For the proof of these properties and more details on the Pfaffian, see, e.g., Ref. [30] and the appendix of Ref. [31].

Consider a symmetry transformation realized by a unitary or anti-unitary operator $\hat{U}_s$ which maps the sp space into itself by a $M \times M$ unitary matrix U_s:

$$\hat{U}_s^\dagger \hat{c}_k \hat{U}_s = \sum_l U_{s\,kl} \hat{c}_l, \tag{24}$$

or in the $2M$-dimensional space,

$$\hat{U}_s^\dagger \begin{pmatrix} \hat{c} \\ \hat{c}^\dagger \end{pmatrix} \hat{U}_s = \begin{pmatrix} U_s & 0 \\ 0 & U_s^* \end{pmatrix} \begin{pmatrix} \hat{c} \\ \hat{c}^\dagger \end{pmatrix} = \mathcal{U}_s \begin{pmatrix} \hat{c} \\ \hat{c}^\dagger \end{pmatrix}, \tag{25}$$

where $\mathcal{U}_s := \mathrm{diag}(U_s, U_s^*)$ is a $2M \times 2M$ unitary matrix. Under the transformation $|\Phi\rangle \to \hat{U}_s |\Phi\rangle$, the generalized density matrix $\mathcal{R}$ transforms as[2]

$$\mathcal{R} \to (\mathcal{U}_s \mathcal{R} \mathcal{U}_s^\dagger)^{(*)}. \tag{26}$$

Here, $(\cdots)^{(*)}$ denotes that the complex conjugate is taken if $\hat{U}_s$ is an anti-unitary operator. Assuming that $\hat{U}_s$ is a symmetry operator of the system, that is $[\hat{H}, \hat{U}_s] = 0$, we find that the HFB Hamiltonian $\mathcal{H}$ transforms in the same way as the generalized density matrix $\mathcal{R}$:

$$\mathcal{H} \to (\mathcal{U}_s \mathcal{H} \mathcal{U}_s^\dagger)^{(*)}. \tag{27}$$

Now suppose that the HFB vacuum $|\Phi\rangle$ is invariant up to a phase under the operation $\hat{U}_s$, i.e. $\hat{U}_s$ is a symmetry operator of the intrinsic system; it follows that

$$\mathcal{H} = (\mathcal{U}_s \mathcal{H} \mathcal{U}_s^\dagger)^{(*)}. \tag{28}$$

When $\hat{U}_s$ is a unitary operator, it leads to $[\mathcal{H}, \mathcal{U}_s] = 0$. This indicates that the HFB Hamiltonian $\mathcal{H}$ is block diagonalized with respect to the conserved quantum numbers associated with the transformation $\hat{U}_s$.

In particular, we are interested in such a $\hat{U}_s$ generated by a Hermitian particle–hole one-particle operator $\hat{S} = \sum_{kl} S_{kl} \hat{c}_k^\dagger \hat{c}_l$: $\hat{U}_s = e^{i\theta\hat{S}}$ or $e^{i\theta\hat{S}}\hat{K}$, where θ is a real parameter and $\hat{K}$ is the complex conjugation operator which leaves the sp basis $|k\rangle = c_k^\dagger |0\rangle$ invariant: $\hat{K}|k\rangle = |k\rangle$. In this case, $U_s = e^{i\theta S}$. In particular, when $\hat{U}_s = e^{i\theta\hat{S}}$, Eq. (28) leads to

$$\left[\mathcal{H}, \begin{pmatrix} e^{i\theta S} & 0 \\ 0 & e^{-i\theta S^*} \end{pmatrix} \right] = 0. \tag{29}$$

If this holds for an arbitrary θ, one sees

$$\left[\mathcal{H}, \begin{pmatrix} S & 0 \\ 0 & -S^* \end{pmatrix} \right] = 0. \tag{30}$$

Note that since the HFB vacuum is always an eigenstate of the number parity operator $\hat{P}_N = e^{i\pi\hat{N}}$, Eq. (29) reduces to a trivial commutation relation $[\mathcal{H}, -I_{2M}] = 0$ when $\hat{S} = \hat{N}$ and $\theta = \pi$.

The HFB equations achieve self-consistency between the densities and the potentials by an iterative process. We are going to discuss here whether the intrinsic symmetry defined in Eq. (28) is affected

[2] Note the property of an anti-unitary operator $\hat{\Theta}$: $(\langle\Phi|\,\hat{\Theta}^\dagger)\,\hat{O}\,(\hat{\Theta}\,|\Phi\rangle) = (\langle\Phi|(\hat{\Theta}^\dagger\hat{O}\hat{\Theta})|\Phi\rangle)^*$.

by the iterations. From Eqs. (26) and (27) the HFB Hamiltonian has the following property as a functional of the generalized density matrix $\mathcal{R}$ for a symmetry $\hat{U}_s$ of the system, as in the case of HF:

$$\left(\mathcal{U}_s\mathcal{H}[\mathcal{R}]\mathcal{U}_s^\dagger\right)^{(*)} = \mathcal{H}\left[(\mathcal{U}_s\mathcal{R}\mathcal{U}_s^\dagger)^{(*)}\right]. \tag{31}$$

This means that if the initial density $\mathcal{R}^{(0)}$ has a certain symmetry, then the mean-field Hamiltonian $\mathcal{H}[\mathcal{R}^{(0)}]$ for the first step of the iteration has it too. The density $\mathcal{R}^{(1)}$ for the next step is found by diagonalization of $\mathcal{H}[\mathcal{R}^{(0)}]$, hence the same symmetry holds. In each step of the iteration, the intrinsic symmetry is thus conserved. Note that the average particle number is fixed at the desired value by adjusting the chemical potential λ in $\mathcal{H}$ throughout the iterations.

2.4. *Time-reversal symmetry and number parity*

Using the results obtained above, we show that the time-reversal symmetry of the HFB Hamiltonian and the number parity of the HFB vacuum are directly related to each other.

Let us consider the case when the HFB Hamiltonian has time-reversal symmetry. Paying attention to the anti-unitarity of the time-reversal operator $\hat{T} = \exp(-i\pi\hat{S}_y)\hat{K}$, where $\hat{S}_y$ is the y-component of the total spin operator, we have the following equality relation from Eq. (28):

$$\mathcal{H} = \mathcal{T}\mathcal{H}^*\mathcal{T}^\mathsf{T}, \tag{32}$$

where

$$\mathcal{T} \coloneqq \begin{pmatrix} T & 0 \\ 0 & T \end{pmatrix}, \qquad T \coloneqq e^{-i\pi S_y} = I_{M/2} \otimes -i\sigma_y = \begin{pmatrix} 0 & -1 & & & & & \\ 1 & 0 & & & & 0 & \\ & & 0 & -1 & & & \\ & & 1 & 0 & & & \\ & & & & \ddots & & \\ & 0 & & & & 0 & -1 \\ & & & & & 1 & 0 \end{pmatrix}. \tag{33}$$

It follows that when φ_k is an eigenvector of $\mathcal{H}$ with eigenvalue E_k, the time-reversed state $\mathcal{T}\varphi_k^*$ is an independent eigenvector of $\mathcal{H}$ with the same eigenvalue E_k. In other words, φ_k and $\mathcal{T}\varphi_k^*$ are degenerate, i.e. the Kramers degeneracy shows up. Since the particle–hole symmetry in Eq. (9) is always kept in HFB theory, $\Sigma_x\varphi_k^*$ and $\Sigma_x\mathcal{T}\varphi_k$ are also Kramers-degenerate eigenvectors with eigenvalue $-E_k$. Therefore, a specific solution of the HFB equations is constructed as follows:

$$\widetilde{\mathcal{W}} = \begin{pmatrix} \widetilde{U} & \widetilde{V}^* \\ \widetilde{V} & \widetilde{U}^* \end{pmatrix}, \tag{34}$$

$$\widetilde{U} = \begin{pmatrix} u_1 & Tu_1^* & u_2 & Tu_2^* & \cdots & u_{M/2} & Tu_{M/2}^* \end{pmatrix}, \tag{35}$$

$$\widetilde{V} = \begin{pmatrix} v_1 & Tv_1^* & v_2 & Tv_2^* & \cdots & v_{M/2} & Tv_{M/2}^* \end{pmatrix}, \tag{36}$$

where $\varphi_k = \binom{u_k}{v_k}$, $\mathcal{T}\varphi_k^* = \binom{Tu_k^*}{Tv_k^*}$, $\Sigma_x\varphi_k^* = \binom{v_k^*}{u_k^*}$, and $\Sigma_x\mathcal{T}\varphi_k = \binom{Tv_k}{Tu_k}$ are orthonormal eigenvectors of $\mathcal{H}$ with eigenvalues E_k, E_k, $-E_k$, and $-E_k$, respectively. Here, we take all E_k non-negative without loss of generality. The orthogonality of φ_k and $\mathcal{T}\varphi_k^*$ is ensured as $\varphi_k^\dagger\mathcal{T}\varphi_k^* = (\varphi_k^\dagger\mathcal{T}\varphi_k^*)^\mathsf{T} =$

$\varphi_k^\dagger \mathcal{T}^\mathsf{T} \varphi_k^* = -\varphi_k^\dagger \mathcal{T} \varphi_k^* = 0$. If $E_k \neq 0$, φ_k is orthogonal to $\Sigma_x \varphi_k^*$ because they are eigenvectors of the same Hermitian matrix with different eigenvalues, and even if $E_k = 0$, it is possible to redefine φ_k to be orthogonal to $\Sigma_x \varphi_k^*$ by mixing φ_k and $\mathcal{T}\varphi_k^*$. Thus, $\widetilde{\mathcal{W}}$ is a unitary matrix. In addition, we find that $\widetilde{\mathcal{W}}$ is a symplectic matrix; that is, it satisfies

$$\widetilde{\mathcal{W}}^\mathsf{T} \mathcal{T} \widetilde{\mathcal{W}} = \mathcal{T}. \tag{37}$$

This is shown as follows: Multiplying both sides of Eq. (35) by T from the left and T^T from the right, we get

$$\begin{aligned} T\widetilde{U}T^\mathsf{T} &= T \begin{pmatrix} u_1 & Tu_1^* & u_2 & Tu_2^* & \cdots & u_{M/2} & Tu_{M/2}^* \end{pmatrix} T^\mathsf{T} \\ &= \begin{pmatrix} Tu_1 & -u_1^* & Tu_2 & -u_2^* & \cdots & Tu_{M/2} & -u_{M/2}^* \end{pmatrix} T^\mathsf{T} \\ &= \begin{pmatrix} u_1^* & Tu_1 & u_2^* & Tu_2 & \cdots & u_{M/2}^* & Tu_{M/2} \end{pmatrix} = \widetilde{U}^*. \end{aligned}$$

In the same way, one obtains $T\widetilde{V}T^\mathsf{T} = \widetilde{V}^*$. Thus, it follows that

$$\mathcal{T}\widetilde{\mathcal{W}}\mathcal{T}^\mathsf{T} = \widetilde{\mathcal{W}}^*. \tag{38}$$

Then, multiplying both sides of Eq. (38) by $\widetilde{\mathcal{W}}^\mathsf{T}$ from the left and $\mathcal{T}$ from the right, and using the fact that $\widetilde{\mathcal{W}}$ is a unitary matrix and $\mathcal{T}$ is an orthogonal matrix, we obtain Eq. (37). It is known that the determinant of any symplectic matrix is $+1$. This is easily shown through the use of Pfaffian: taking the Pfaffian of both sides of Eq. (37), it follows that $\det \widetilde{\mathcal{W}}\, \mathrm{pf}\, \mathcal{T} = \mathrm{pf}\, \mathcal{T}$, and since $\mathrm{pf}\, \mathcal{T} = (-1)^M \neq 0$, one sees

$$\det \widetilde{\mathcal{W}} = +1. \tag{39}$$

Now the HFB equations are written as

$$\widetilde{\mathcal{W}}^\dagger \mathcal{H} \widetilde{\mathcal{W}} = \widetilde{\mathcal{E}}, \tag{40}$$

where $\widetilde{\mathcal{E}} = \mathrm{diag}(\tilde{E}, -\tilde{E})$ and $\tilde{E} = \mathrm{diag}(E_1, E_1, E_2, E_2, \ldots, E_{M/2}, E_{M/2})$. From Eqs. (21) and (39) we have

$$\mathrm{pf}\, \mathcal{H}_\mathcal{X} = \prod_{k=1}^{M/2} E_k^2. \tag{41}$$

It follows that $\mathrm{pf}\, \mathcal{H}_\mathcal{X} \geq 0$, with equality if $E_k = 0$ for at least one k. This, together with Eq. (23), means that the lowest-energy solution of the HFB equations has even number parity as long as the time-reversal symmetry is conserved in the HFB Hamiltonian with no null eigenvalues.

Next, we show that the lowest-energy state is not well defined when the HFB Hamiltonian has null eigenvalues. A general solution of the HFB equations under the time-reversal symmetry is obtained by

$$\mathcal{W} = \widetilde{\mathcal{W}} \mathcal{Z}, \tag{42}$$

where $\mathcal{Z}$ is a $2M \times 2M$ unitary matrix which consists of the unitary transformations containing the permutation of columns as well as the phase transformation and mixing of the degenerate qp states. From Eqs. (15), (39), and (42), the number parity of the state under consideration is now given by $\pi_N = \det \mathcal{Z}$. Only the permutation of the kth and $(M+k)$th columns ($k \leq M$), that is, a quasi-particle state with eigenvalue E_k and the corresponding quasi-hole state with eigenvalue $-E_k$, changes the number parity. This is because, for $\mathcal{W}$ to be written in the form of Eq. (2), the permutation of the kth and lth columns ($k < l \leq M$) accompanies the permutation of the $(M+k)$th and $(M+l)$th columns, and no other permutations except that of the kth and $(M+k)$th columns are allowed. For the lowest-energy state, however, the permutation of the quasi-particle and quasi-hole states is permitted only if $E_k = 0$, because the permutation means swapping of E_k and $-E_k$ and goes against the definition of the lowest-energy state unless $E_k = 0$. When $E_k = 0$, any mixing of φ_k, $\mathcal{T}\varphi_k^*$, $\Sigma_x\varphi_k^*$, and $\Sigma_x\mathcal{T}\varphi_k$, or the kth, $(k+1)$th, $(M+k)$th, and $(M+k+1)$th columns, is allowed for the lowest-energy state since they are all degenerate, and such a mixing can change the number parity of the lowest-energy state as discussed above. Therefore, we cannot uniquely determine the lowest-energy state with a specific number parity when the HFB Hamiltonian has null eigenvalues.

Finally, we would like to make sure that the above conclusion is not broken via nonlinear effects. If the HFB Hamiltonian does not have null eigenvalues, there is no mixing between quasi-particle and quasi-hole states for the lowest-energy state. Thus, the lowest-energy solution $\mathcal{W}_{\rm LE}$ is written as

$$\mathcal{W}_{\rm LE} = \widetilde{\mathcal{W}} \begin{pmatrix} X & 0 \\ 0 & X^* \end{pmatrix}, \tag{43}$$

where X is a $M \times M$ unitary matrix. Then, $\det \mathcal{W}_{\rm LE} = |\det X|^2 = +1$, and we get the above conclusion again: the lowest-energy solution of the HFB equation has even number parity as long as the time-reversal symmetry is conserved in the HFB Hamiltonian without null eigenvalues. From Eq. (5), the generalized density matrix for the lowest-energy state is obtained by

$$\mathcal{R}_{\rm LE} = \mathcal{W}_{\rm LE} \begin{pmatrix} O_M & O_M \\ O_M & I_M \end{pmatrix} \mathcal{W}_{\rm LE}^\dagger = \widetilde{\mathcal{W}} \begin{pmatrix} O_M & O_M \\ O_M & I_M \end{pmatrix} \widetilde{\mathcal{W}}^\dagger. \tag{44}$$

From Eq. (38), this $\mathcal{R}_{\rm LE}$ has the time-reversal symmetry:

$$\mathcal{T}\mathcal{R}_{\rm LE}^*\mathcal{T}^{\mathsf{T}} = \mathcal{R}_{\rm LE}. \tag{45}$$

Therefore, from the discussion in Sect. 2.3, the lowest-energy state constructed as Eq. (43) has even number parity at each step of the iteration.

3. Methodology for describing odd-mass nuclei

We demonstrated above that the lowest-energy state is always an even number-parity state, that is, an even particle system, in HFB theory as long as the time-reversal symmetry is conserved for the intrinsic Hamiltonian. The procedure called the blocking method, which has conventionally been used to describe an odd number-parity state [12,21,34], can be viewed as follows: One solves the time-reversal symmetric HFB equations to generate a reference state with $\det \mathcal{W} = +1$, and then swaps one set of columns of $\mathcal{W}$ to obtain a state whose determinant sign is reversed. Alternatively, one can use the strategy of describing an odd number-parity state as the lowest-energy state under

the constraint which breaks time-reversal symmetry. The difference between our method and the blocking method is explained in Eq. (22). In the blocking method, to change the number parity π_N one replaces E_k by $-E_k$ for a certain k on the right-hand side of Eq. (22), leaving pf $\mathcal{H}_\mathcal{X}$ as it is. In our method, on the other hand, we change the sign of pf $\mathcal{H}_\mathcal{X}$ by a time-odd constraint while keeping the sign of the right-hand side to change π_N. The idea of obtaining odd-mass nuclei by such a constraint was proposed by Bertsch et al., stimulated by the non-collective cranking method [24]. In what follows, we generalize this approach and encapsulate the essential point of this method.

Assuming that the intrinsic system is invariant under any unitary transformation generated by a Hermitian time-odd particle–hole-type one-body operator, $\hat{S} = \sum_{ij} S_{ij} c_i^\dagger c_j$ with $S^\dagger = S$, and $TS^*T^\mathsf{T} = -S$. For example, the z-component of the total angular momentum $\hat{J}_z$ can be employed as $\hat{S}$ for an axially symmetric system around the z-axis. Since $\hat{S}$ is a symmetry of the intrinsic system, the mean-field representation of $\hat{S}$ commutes with the HFB Hamiltonian $\mathcal{H}$ [see Eq. (30)]:

$$[\mathcal{H}, \mathcal{S}] = 0, \tag{46}$$

where

$$\mathcal{S} = \begin{pmatrix} S & 0 \\ 0 & -S^* \end{pmatrix}. \tag{47}$$

Introducing a Lagrange multiplier λ_s to fix the expectation value of $\hat{S}$ along with the chemical potential λ, we consider the variational principle

$$\delta \langle \hat{H} - \lambda \hat{N} - \lambda_s \hat{S} \rangle = 0. \tag{48}$$

This then gives the HFB Routhian

$$\mathcal{H}' = \mathcal{H} - \lambda_s \mathcal{S}. \tag{49}$$

From the commutation relation in Eq. (46), $\mathcal{H}$ can be block diagonalized for each eigenvalue of $\mathcal{S}$. Since $\mathcal{S}$ is proportional to the identity matrix in each block, the eigenvalues of $\mathcal{H}'$ are linearly shifted from those of $\mathcal{H}$. Then, as shown below, the sign of pf $\mathcal{H}'_\mathcal{X}$ can change according to λ_s, and thus the number parity of the lowest-energy state can vary from positive to negative.

Because of the time-odd character of $\hat{S}$, the eigenvalues of S always come in pairs of opposite signs. Let $\{x_n^{\pm\alpha}\}_{n=1,2,\ldots}$ be sets of orthonormalized eigenvectors of S with eigenvalues $\pm\omega_\alpha$ ($\alpha > 0$, $\omega_\alpha > 0$), where n is a label that distinguishes states other than α. Then,

$$\left\{ \begin{pmatrix} x_n^\alpha \\ 0 \end{pmatrix}, \begin{pmatrix} 0 \\ x_n^{-\alpha *} \end{pmatrix} \right\}_{n=1,2,\ldots} \tag{50}$$

is a set of orthonormalized eigenvectors of $\mathcal{S}$ with eigenvalue ω_α. An appropriate linear combination

$$\chi_n^\alpha = \sum_m \left[U_{mn}^\alpha \begin{pmatrix} x_m^\alpha \\ 0 \end{pmatrix} + V_{mn}^\alpha \begin{pmatrix} 0 \\ x_m^{-\alpha *} \end{pmatrix} \right] \tag{51}$$

is a simultaneous eigenstate of $\mathcal{S}$ and $\mathcal{H}$ with an eigenvalue ω_α and E_n^α, respectively. Thanks to the particle–hole symmetry of $\mathcal{H}$,

$$\varphi_n^\alpha \coloneqq \Sigma_x \left(\chi_n^{-\alpha}\right)^* = \sum_m \left[V_{mn}^{-\alpha *} \begin{pmatrix} x_m^\alpha \\ 0 \end{pmatrix} + U_{mn}^{-\alpha *} \begin{pmatrix} 0 \\ x_m^{-\alpha *} \end{pmatrix} \right] \tag{52}$$

is also a simultaneous eigenstate of $\mathcal{S}$ and $\mathcal{H}$ with an eigenvalue ω_α and $-E_n^{-\alpha}$, respectively. Therefore, the HFB equations are block diagonalized for each eigenvalue of $\mathcal{S}$ as follows:

$$\mathcal{W}^{\alpha\dagger}\mathcal{H}^\alpha\mathcal{W}^\alpha = \mathcal{E}^\alpha, \tag{53}$$

where

$$\mathcal{H}^\alpha = \begin{pmatrix} (h-\lambda I)^\alpha & \Delta^\alpha \\ -\Delta^{-\alpha *} & -(h-\lambda I)^{-\alpha *} \end{pmatrix}, \quad \mathcal{W}^\alpha = \begin{pmatrix} U^\alpha & V^{-\alpha *} \\ V^\alpha & U^{-\alpha *} \end{pmatrix}, \quad \mathcal{E}^\alpha = \begin{pmatrix} E^\alpha & 0 \\ 0 & -E^{-\alpha} \end{pmatrix}, \tag{54}$$

and

$$(h-\lambda I)^\alpha_{mn} = x_m^{\alpha\dagger}(h-\lambda I_M)x_n^\alpha, \qquad \Delta^\alpha_{mn} = x_m^{\alpha\dagger}\Delta x_n^{-\alpha *}, \qquad E^\alpha = \mathrm{diag}(E_1^\alpha, E_2^\alpha, \ldots). \tag{55}$$

Since χ_n^α and φ_n^α are simultaneous eigenstates of $\mathcal{S}$ and $\mathcal{H}$, they are also eigenstates of $\mathcal{H}'$ with eigenvalue $E_n^\alpha - \lambda_s\omega_\alpha$ and $-E_n^{-\alpha} - \lambda_s\omega_\alpha$, respectively. In other words,

$$\mathcal{W}^{\alpha\dagger}\mathcal{H}'^\alpha\mathcal{W}^\alpha = \mathcal{E}^\alpha - \lambda_s\omega_\alpha I^\alpha, \tag{56}$$

where $\mathcal{H}'^\alpha = \mathcal{H}^\alpha - \lambda_s\omega_\alpha I^\alpha$, and I^α is the identity matrix for the block with eigenvalue ω_α. In this way, one sees that the constraint on the intrinsic symmetry $\hat{S}$ does not change individual single-qp states, but shifts only the qp energies according to the eigenvalues of $\mathcal{S}$. Reflecting the time-odd character of $\hat{S}$, the qp energies of time-reversal pairs split in the opposite direction. Therefore, even if the original HFB Hamiltonian $\mathcal{H}$ has time-reversal symmetry, the Kramers degeneracy is resolved at $\lambda_s \neq 0$.

We now show that the number parity of the lowest-energy state can change according to λ_s. The following unitary matrix diagonalizes $\mathcal{H}$ and $\mathcal{H}'$ simultaneously:

$$\underline{\mathcal{W}} = \begin{pmatrix} \underline{U} & \underline{V}^* \\ \underline{V} & \underline{U}^* \end{pmatrix}, \tag{57}$$

$$\underline{U} = \begin{pmatrix} \underline{U}^1 & \underline{U}^{-1} & \underline{U}^2 & \underline{U}^{-2} & \cdots \end{pmatrix}, \qquad \underline{U}_n^\alpha = \sum_m x_m^\alpha U_{mn}^\alpha, \tag{58}$$

$$\underline{V} = \begin{pmatrix} \underline{V}^1 & \underline{V}^{-1} & \underline{V}^2 & \underline{V}^{-2} & \cdots \end{pmatrix}, \qquad \underline{V}_n^\alpha = \sum_m x_m^{-\alpha *} V_{mn}^\alpha. \tag{59}$$

Then, the HFB equations for $\mathcal{H}$ and $\mathcal{H}'$ read

$$\underline{\mathcal{W}}^\dagger\mathcal{H}\underline{\mathcal{W}} = \underline{\mathcal{E}}, \qquad \underline{\mathcal{W}}^\dagger\mathcal{H}'\underline{\mathcal{W}} = \underline{\mathcal{E}}', \tag{60}$$

where $\underline{\mathcal{E}} = \mathrm{diag}\,(\underline{E}, -\underline{E})$, $\underline{E} = \mathrm{diag}\,(E^1, E^{-1}, \ldots)$, and $\underline{\mathcal{E}}' = \mathrm{diag}\,(\underline{E}', -\underline{E}')$, $\underline{E}' = \mathrm{diag}\,(E^1 - \lambda_s\omega_1 I^1, E^{-1} + \lambda_s\omega_1 I^1, \ldots)$. From Eq. (21) one obtains

$$\det \underline{\mathcal{W}}\,\mathrm{pf}\,\mathcal{H}_\mathcal{X} = \prod_{n,\alpha>0} E_n^\alpha E_n^{-\alpha}, \tag{61}$$

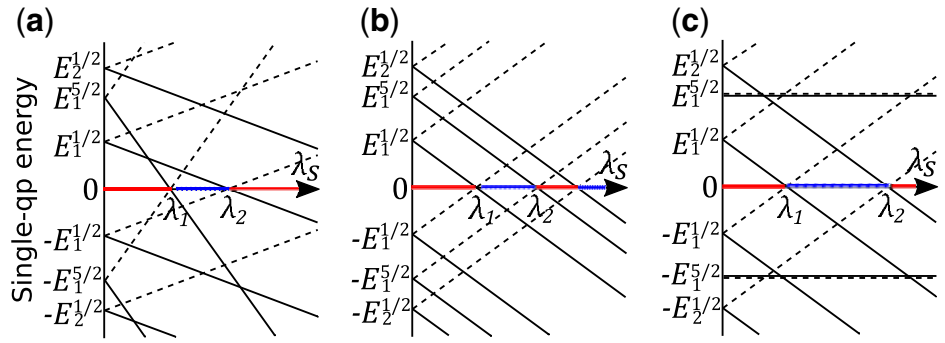

Fig. 1. Schematic picture of the single-qp levels with $\hat{J}_z$ eigenvalues Ω ($\Omega > 0$: solid line; $\Omega < 0$: dashed line) as functions of the parameter λ_s for the cases employing the operator (a) $\hat{J}_z$, (b) $\hat{J}_z/|J_z|$, and (c) $|J_z = 1/2\rangle\langle J_z = 1/2| - |J_z = -1/2\rangle\langle J_z = -1/2|$ as the constraint operator $\hat{S}$. Twelve levels with $|\Omega| = 1/2^2, 5/2$ are shown. At $\lambda_s = 0$, the nth lowest (positive) single-qp energies with $\pm\Omega$ are degenerate and displayed as E_n^{Ω}. With increasing λ_s, the number parity of the lowest-energy state keeps $+1$ for $\lambda_s < \lambda_1$, the sign changes at $\lambda_s = \lambda_1$, and the number parity is -1 for $\lambda_1 < \lambda_s < \lambda_2$.

$$\det \underline{\mathcal{W}} \,\mathrm{pf}\, \mathcal{H}'_{\mathcal{X}} = \prod_{n,\alpha>0} (E_n^{\alpha} - \lambda_s \omega_{\alpha})(E_n^{-\alpha} + \lambda_s \omega_{\alpha}). \tag{62}$$

When the original HFB Hamiltonian $\mathcal{H}$ is time-reversal symmetric, from Eq. (41) one obtains

$$\mathrm{pf}\, \mathcal{H}_{\mathcal{X}} = \prod_{n,\alpha>0} (E_n^{\alpha})^2. \tag{63}$$

Substituting this into Eq. (61), together with $E_n^{\alpha} = E_n^{-\alpha}$, one sees that

$$\det \underline{\mathcal{W}} = +1. \tag{64}$$

Substituting this into Eq. (62), one sees that

$$\mathrm{pf}\, \mathcal{H}'_{\mathcal{X}} = \prod_{n,\alpha>0} \left[(E_n^{\alpha})^2 - (\lambda_s \omega_{\alpha})^2\right]. \tag{65}$$

Therefore, from Eq. (23) the number parity of the lowest-energy state under the constraint is given by

$$\pi_N^{\mathrm{LE}} = \prod_{n,\alpha>0} \mathrm{sgn}\left[(E_n^{\alpha})^2 - (\lambda_s \omega_{\alpha})^2\right]. \tag{66}$$

At $\lambda_s = 0$, $\pi_N^{\mathrm{LE}} = +1$, namely the lowest-energy state has even number parity. For $\lambda_s \neq 0$, the number parity changes according to the magnitude relation between E_n^{α} and $\lambda_s \omega_{\alpha}$. The number parity of the lowest-energy state thus changes according to the magnitude of λ_s.

Figure 1 shows a schematic picture of the single-qp energies under the constraint. When λ_s is set to an appropriate value $\lambda_1 < \lambda_s < \lambda_2$, where a pair of levels intersect the axis at $\lambda_s = \lambda_1$, an odd number-parity state is automatically obtained as the lowest-energy state. Determined by the operator $\hat{S}$ are the orbital whose qp energy changes with an increase in λ_s and the level which intersects the axis first. In this sense $\hat{S}$ is considered as a selector of the vacuum. Note that when two levels cut across the axis by increasing λ_s, the number parity of the system becomes even, corresponding to the two-qp excitation state. Specifically, when the z-component of the total angular momentum $\hat{J}_z$

is a symmetry of the intrinsic system, different vacuums are selected depending on the choice of $\hat{S}$. We consider three cases:

Case (i): When $\hat{J}_z$ itself is taken as $\hat{S}$, each qp level rises or falls with the slope of the corresponding eigenvalue $J_z = \Omega$, see Fig. 1(a). As λ_s increases, the orbital with high Ω is preferably selected as the level to be excited. This is equivalent to the so-called non-collective cranking, where particles with high angular momentum about the symmetry axis are aligned.

Case (ii): Let us look at the case of using $\hat{J}_z/|J_z|$ as $\hat{S}$. Since $\hat{J}_z/|J_z|$ is an operator that gives $+1$ for eigenstates with positive Ω and -1 for eigenstates with negative Ω, each qp level separates out with a slope of ± 1 independent of the magnitude of Ω with an increase in λ_s, see Fig. 1(b). Therefore, in this case, an orbital with a smaller qp energy is likely to be selected as the level to be excited. This corresponds to the "two-Fermi level approach" proposed in Ref. [24]. As mentioned in Ref. [24], this choice may not work well for the case in which the single-qp level density is high near the Fermi level and the spherical systems where we have $(2j + 1)$-folded degeneracy. Introducing a kind of projection operator was conjectured in Ref. [24] to resolve the issue, and we realize the practical method in the following case.

Case (iii): Let us consider the case of using a time-odd projection operator $|J_z = \Omega\rangle \langle J_z = \Omega| - |J_z = -\Omega\rangle \langle J_z = -\Omega|$ as $\hat{S}$. This is a part of $\hat{J}_z/|J_z|$, and is an operator which works only for the state with a certain Ω. Therefore, in this case, only the level carrying the specified eigenvalue $\pm\Omega$ splits for $\lambda_s \neq 0$, and the levels having other eigenvalues of $\hat{J}_z$ do not change even if λ_s increases, see Fig. 1(c). Thus, one can select the state of interest easily. The third choice is convenient for practical use and we perform the calculations using this choice in the following investigation.

We have generalized the method proposed in Ref. [24] with a generic time-odd operator $\hat{S}$, and then proposed a practical choice for $\hat{S}$ of a time-odd projection operator. In Ref. [24] the authors concluded that their approach had some difficulties compared with the conventional blocking method:

- Not all the qp states are easily accessible in their approach, and it describes only the specific configurations.
- The method fails to describe a one-qp state when qp levels show degeneracies beyond the Kramers degeneracy.
- The self-consistent calculations in a high qp-level density near the Fermi surface lead to numerical instabilities.

Our generalization and practical application of the method overcome these difficulties in some cases. Even when additional degeneracies are present beyond the Kramers degeneracy, our practical method gives a one-qp state with a desired quantum number as long as the $\hat{S}$ completely lifts those degeneracies, and the numerical instabilities can be less severe because the qp-level densities change with increasing λ_s depending on the choice of $\hat{S}$. For instance, when $(2j + 1)$-fold degeneracy is present in a spherical nucleus, one can selectively lower the single-particle energies of qp levels with a certain Ω to get the one-qp state with the quantum number. In neutron-drip-line nuclei, however, a high density of state near the Fermi level causes numerical instability as in the usual blocking method. Compared to the conventional blocking method, our method has the advantage of being easy to code for calculating odd-mass nuclei: all we have to do is to add the identity matrix with an appropriate coefficient to the HFB Hamiltonian, as will be seen in detail in the next section, and then

odd-mass nuclei are calculated as the lowest-energy solution of the HFB equation just like even–even nuclei.

4. Numerical analysis for deformed neutron-rich Mg isotopes

4.1. HFB equation for axially symmetric nuclei with time-even and time-odd mean fields

The coordinate-space HFB equation obtained by employing the local EDF containing time-even and time-odd parts reads [35,36]

$$\sum_{\sigma'=\pm\frac{1}{2}} \begin{bmatrix} h^q_{\sigma\sigma'}(\boldsymbol{r}) - \lambda^q \delta_{\sigma\sigma'} & \tilde{h}^q_{\sigma\sigma'}(\boldsymbol{r}) \\ 4\sigma\sigma' \tilde{h}^{q*}_{-\sigma-\sigma'}(\boldsymbol{r}) & -4\sigma\sigma' h^{q*}_{-\sigma-\sigma'}(\boldsymbol{r}) + \lambda^q \delta_{\sigma\sigma'} \end{bmatrix} \begin{bmatrix} \varphi^q_{1,i}(\boldsymbol{r}\,\sigma') \\ \varphi^q_{2,i}(\boldsymbol{r}\,\sigma') \end{bmatrix} = E^q_i \begin{bmatrix} \varphi^q_{1,i}(\boldsymbol{r}\,\sigma) \\ \varphi^q_{2,i}(\boldsymbol{r}\,\sigma) \end{bmatrix}, \tag{67}$$

where q stands for protons (p) and neutrons (n), in which the quasiparticles are assumed to be eigenstates of the third component of the isospin operator. The sp Hamiltonian h consists of the mean-field (Kohn–Sham) potentials Γ_t composed of the time-even and time-odd isoscalar ($t = 0$) and isovector ($t = 1$) densities as

$$h^{\mathrm{n}}_{\sigma\sigma'} = \left[-\frac{\hbar^2}{2m} \triangle + \Gamma^{\mathrm{even}}_0 + \Gamma^{\mathrm{odd}}_0 + \Gamma^{\mathrm{even}}_1 + \Gamma^{\mathrm{odd}}_1 \right]_{\sigma\sigma'}, \tag{68}$$

$$h^{\mathrm{p}}_{\sigma\sigma'} = \left[-\frac{\hbar^2}{2m} \triangle + \Gamma^{\mathrm{even}}_0 + \Gamma^{\mathrm{odd}}_0 - \Gamma^{\mathrm{even}}_1 - \Gamma^{\mathrm{odd}}_1 + V_{\mathrm{Coul}} \right]_{\sigma\sigma'}. \tag{69}$$

Here, V_{Coul} is the Coulomb potential, and the explicit expressions for Γ for the Skyrme-type EDF are shown in the Appendix. Thanks to the time-reversal (anti)symmetry of the potentials, one sees

$$\bar{h}^{\mathrm{n}}_{\sigma\sigma'} \coloneqq 4\sigma\sigma' h^{\mathrm{n}*}_{-\sigma-\sigma'} = \left[-\frac{\hbar^2}{2m} \triangle + \Gamma^{\mathrm{even}}_0 - \Gamma^{\mathrm{odd}}_0 + \Gamma^{\mathrm{even}}_1 - \Gamma^{\mathrm{odd}}_1 \right]_{\sigma\sigma'}, \tag{70}$$

$$\bar{h}^{\mathrm{p}}_{\sigma\sigma'} \coloneqq 4\sigma\sigma' h^{\mathrm{p}*}_{-\sigma-\sigma'} = \left[-\frac{\hbar^2}{2m} \triangle + \Gamma^{\mathrm{even}}_0 - \Gamma^{\mathrm{odd}}_0 - \Gamma^{\mathrm{even}}_1 + \Gamma^{\mathrm{odd}}_1 + V_{\mathrm{Coul}} \right]_{\sigma\sigma'}. \tag{71}$$

We employ the pairing EDF that contains only the time-even densities as described below, so that we see

$$4\sigma\sigma' \tilde{h}^{q*}_{-\sigma-\sigma'} = \tilde{h}^q_{\sigma\sigma'}. \tag{72}$$

We solve the HFB equation in Eq. (67) by assuming axial and reflection symmetries so that the quasiparticles are labeled by $\{\Omega, \pi, q\}$, with Ω and π being the z-component of the total angular momentum and parity, respectively. In this case, the qp wave functions can be written in the form

$$\varphi^q_{a,n\Omega\pi}(\boldsymbol{r}\,\sigma) = \varphi^{q+}_{a,n\Omega\pi}(\varrho, z)\, e^{i\Lambda^- \phi} \chi_{1/2}(\sigma) + \varphi^{q-}_{a,n\Omega\pi}(\varrho, z)\, e^{i\Lambda^+ \phi} \chi_{-1/2}(\sigma) \qquad (a = 1, 2), \tag{73}$$

where $\Lambda^\pm = \Omega \pm 1/2$ [37], and ϱ, z, and ϕ are the cylindrical coordinates defining the three-dimensional position vector as $\boldsymbol{r} = (\varrho\cos\phi, \varrho\sin\phi, z)$, while z is the chosen symmetry axis. Also, the wave functions satisfy the following symmetry:

$$\varphi^{q\pm}_{a,n\Omega\pi}(\varrho, -z) = \pi(-1)^{\Lambda^\mp} \varphi^{q\pm}_{a,n\Omega\pi}(\varrho, z) \qquad (a = 1, 2). \tag{74}$$

The coordinate-space HFB equation has been solved under the assumption of axial symmetry in many cases; however, time-reversal symmetry is often imposed [38–42]. To keep the present paper

self-contained, the mean-field potentials containing both the time-even and time-odd densities and currents in the cylindrical-coordinate representation are shown in the Appendix. With the axial symmetry, the ϕ dependencies of the sp and pair Hamiltonians are given by

$$h^q(\boldsymbol{r}) = \begin{bmatrix} h^q_{\uparrow\uparrow}(\varrho,z;l_z) & e^{-i\phi}h^q_{\uparrow\downarrow}(\varrho,z;l_z) \\ e^{i\phi}h^q_{\downarrow\uparrow}(\varrho,z;l_z) & h^q_{\downarrow\downarrow}(\varrho,z;l_z) \end{bmatrix}, \quad \bar{h}^q(\boldsymbol{r}) = \begin{bmatrix} \bar{h}^q_{\uparrow\uparrow}(\varrho,z;l_z) & e^{-i\phi}\bar{h}^q_{\uparrow\downarrow}(\varrho,z;l_z) \\ e^{i\phi}\bar{h}^q_{\downarrow\uparrow}(\varrho,z;l_z) & \bar{h}^q_{\downarrow\downarrow}(\varrho,z;l_z) \end{bmatrix}, \tag{75}$$

and

$$\tilde{h}^q(\boldsymbol{r}) = \begin{bmatrix} \tilde{h}^q_{\uparrow\uparrow}(\varrho,z;l_z) & e^{-i\phi}\tilde{h}^q_{\uparrow\downarrow}(\varrho,z;l_z) \\ e^{i\phi}\tilde{h}^q_{\downarrow\uparrow}(\varrho,z;l_z) & \tilde{h}^q_{\downarrow\downarrow}(\varrho,z;l_z) \end{bmatrix}, \tag{76}$$

where $l_z = \frac{\partial_\phi}{i}$, and thus the HFB equation in the (ϱ,z) space for each $\{\Omega,\pi,q\}$ reads

$$\begin{pmatrix} h^{\Omega\pi q}_{\uparrow\uparrow}-\lambda^q & h^{\Omega\pi q}_{\uparrow\downarrow} & \tilde{h}^{\Omega\pi q}_{\uparrow\uparrow} & \tilde{h}^{\Omega\pi q}_{\uparrow\downarrow} \\ h^{\Omega\pi q}_{\downarrow\uparrow} & h^{\Omega\pi q}_{\downarrow\downarrow}-\lambda^q & \tilde{h}^{\Omega\pi q}_{\downarrow\uparrow} & \tilde{h}^{\Omega\pi q}_{\downarrow\downarrow} \\ \tilde{h}^{\Omega\pi q}_{\uparrow\uparrow} & \tilde{h}^{\Omega\pi q}_{\uparrow\downarrow} & -\bar{h}^{\Omega\pi q}_{\uparrow\uparrow}+\lambda^q & -\bar{h}^{\Omega\pi q}_{\uparrow\downarrow} \\ \tilde{h}^{\Omega\pi q}_{\downarrow\uparrow} & \tilde{h}^{\Omega\pi q}_{\downarrow\downarrow} & -\bar{h}^{\Omega\pi q}_{\downarrow\uparrow} & -\bar{h}^{\Omega\pi q}_{\downarrow\downarrow}+\lambda^q \end{pmatrix} \begin{pmatrix} \varphi^{q+}_{1,n\Omega\pi} \\ \varphi^{q-}_{1,n\Omega\pi} \\ \varphi^{q+}_{2,n\Omega\pi} \\ \varphi^{q-}_{2,n\Omega\pi} \end{pmatrix} = E^q_{n\Omega\pi} \begin{pmatrix} \varphi^{q+}_{1,n\Omega\pi} \\ \varphi^{q-}_{1,n\Omega\pi} \\ \varphi^{q+}_{2,n\Omega\pi} \\ \varphi^{q-}_{2,n\Omega\pi} \end{pmatrix}, \tag{77}$$

where $h^{\Omega\pi q}_{ss'}$, $\bar{h}^{\Omega\pi q}_{ss'}$, and $\tilde{h}^{\Omega\pi q}_{ss'}$ are defined using $\Lambda_\uparrow \coloneqq \Lambda^-$ and $\Lambda_\downarrow \coloneqq \Lambda^+$ as $h^{\Omega\pi q}_{ss'}(\varrho,z) \coloneqq h^q_{ss'}(\varrho,z;l_z=\Lambda_{s'})$, $\bar{h}^{\Omega\pi q}_{ss'}(\varrho,z) \coloneqq \bar{h}^q_{ss'}(\varrho,z;l_z=\Lambda_{s'})$, and $\tilde{h}^{\Omega\pi q}_{ss'}(\varrho,z) \coloneqq \tilde{h}^q_{ss'}(\varrho,z;l_z=\Lambda_{s'})$.

To describe odd-A isotopes, we employ the time-odd projection operator to the states with a specific $\{\Omega,\pi,q\}$ quantum number, $|\Omega\,\pi\,q\rangle\langle\Omega\,\pi\,q| - |-\Omega\,\pi\,q\rangle\langle-\Omega\,\pi\,q|$, as the constraint operator $\hat{S}$. In other words, we introduce the Lagrange multiplier λ_s for the specified $\{\Omega,\pi,q\}$ sector of the HFB equation in Eq. (77) as

$$\begin{pmatrix} h^{\Omega\pi q}_{\uparrow\uparrow}-\lambda^q-\lambda_s & h^{\Omega\pi q}_{\uparrow\downarrow} & \tilde{h}^{\Omega\pi q}_{\uparrow\uparrow} & \tilde{h}^{\Omega\pi q}_{\uparrow\downarrow} \\ h^{\Omega\pi q}_{\downarrow\uparrow} & h^{\Omega\pi q}_{\downarrow\downarrow}-\lambda^q-\lambda_s & \tilde{h}^{\Omega\pi q}_{\downarrow\uparrow} & \tilde{h}^{\Omega\pi q}_{\downarrow\downarrow} \\ \tilde{h}^{\Omega\pi q}_{\uparrow\uparrow} & \tilde{h}^{\Omega\pi q}_{\uparrow\downarrow} & -\bar{h}^{\Omega\pi q}_{\uparrow\uparrow}+\lambda^q-\lambda_s & -\bar{h}^{\Omega\pi q}_{\uparrow\downarrow} \\ \tilde{h}^{\Omega\pi q}_{\downarrow\uparrow} & \tilde{h}^{\Omega\pi q}_{\downarrow\downarrow} & -\bar{h}^{\Omega\pi q}_{\downarrow\uparrow} & -\bar{h}^{\Omega\pi q}_{\downarrow\downarrow}+\lambda^q-\lambda_s \end{pmatrix} \begin{pmatrix} \varphi^{q+}_{1,n\Omega\pi} \\ \varphi^{q-}_{1,n\Omega\pi} \\ \varphi^{q+}_{2,n\Omega\pi} \\ \varphi^{q-}_{2,n\Omega\pi} \end{pmatrix}$$
$$= \left(E^q_{n\Omega\pi}-\lambda_s\right) \begin{pmatrix} \varphi^{q+}_{1,n\Omega\pi} \\ \varphi^{q-}_{1,n\Omega\pi} \\ \varphi^{q+}_{2,n\Omega\pi} \\ \varphi^{q-}_{2,n\Omega\pi} \end{pmatrix}. \tag{78}$$

Here, the chemical potential for protons or neutrons, λ^q, is adjusted so that the average particle number has the desired value, i.e. an odd number for odd-A nuclei. We call the introduction of λ_s "blocking" since this procedure is equivalent to the traditional blocking method.

4.2. Numerical procedures

We solve Eq. (77) by diagonalizing the HFB Hamiltonian in the cylindrical-coordinate representation with the box boundary condition. We discretize the coordinates by $\varrho_i = (i-1/2)\times h$ $(i=1,2,\ldots,N_\rho)$ and $z_j = (j-1)\times h$ $(j=1,2,\ldots,N_z)$, with a lattice mesh size $h = 0.8$ fm, and use 30 points for N_ρ and N_z. Consequently, a qp wave function is expressed as a vector whose dimension is $N = 4N_\rho N_z = 3600$, and the HFB Hamiltonian is a matrix of size $N\times N$. The qp

states are truncated according to the qp energy cutoff at 60 MeV, and the qp states up to $\Omega = 15/2$ with positive and negative parities are included. The differential operators are represented by use of the 13-point formula of the finite difference method. For diagonalization of the Hamiltonian or Routhian we use the LAPACK DSYEVX subroutine [43]. A modified Broyden's method [44] is utilized to calculate new densities during the self-consistent iteration. We consider that the calculation converges when both the difference of the total energy (in MeV) between two consecutive iterations and the deviations of the calculated particle numbers from the desired neutron and proton numbers become smaller than 10^{-4}. The Lagrange multiplier λ_s is adjusted to $\lambda_s = (E^q_{1\Omega\pi} + E^q_{2\Omega\pi})/2$, where $E^q_{1\Omega\pi}$ and $E^q_{2\Omega\pi}$ are the lowest and the second lowest positive qp energies for the given $\{\Omega, \pi, q\}$ at each iteration, so that only one pair of qp levels intersect the energy-zero axis.

For the normal (particle–hole) part of a nuclear EDF, we employ the SLy4 functional [45]. The so-called naïve choice [12] is adopted for determining the coupling constants of the time-odd terms in the EDF, except that the coupling constants of the terms of the form $\boldsymbol{s}\cdot\triangle\boldsymbol{s}$, where $\boldsymbol{s}$ is the spin density, are set to zero because these terms in some cases lead to divergences of the HFB iterative procedure [12]. For the particle–particle channel, we adopt the density functional in Eq. (A.30) which corresponds to the density-dependent contact interaction. The parameters are set as $V_1 = 1$ and $\gamma = 1$ (surface pairing), and the pairing strength is taken as $V_0 = -430\,\text{MeV fm}^3$ to approximately reproduce the experimental pairing gap of neutrons (1.28 MeV based on AME2016 [46]) of ^{35}Mg. The pairing gap is obtained by use of the three-point formula for the binding energy [47], and the calculated $\Delta^{(3)}_{\text{n}}$ for ^{35}Mg is found to be 1.47 MeV.

4.3. Numerical results and discussion

To demonstrate the feasibility of our method, we performed the systematic calculation for the neutron-rich Mg isotopes with mass number $A = 34$–40. We excluded ^{32}Mg and ^{33}Mg in the present investigation, where the loss of spherical magic number of 20 has been under debate, because the shape fluctuation and the correlation beyond the mean-field approximation may be significant in ^{32}Mg [48–50], and many-particle many-hole states with different shape deformation may coexist in ^{33}Mg [51,52], as mentioned slightly below.

We tried blocking each of $\Omega^\pi = 1/2^\pm$, $3/2^\pm$, $5/2^\pm$, and $7/2^\pm$ orbitals for odd-mass isotopes, and the ground state was obtained by blocking the orbital with $\Omega^\pi = 3/2^-$, $5/2^-$, and $1/2^-$ in ^{35}Mg, ^{37}Mg, and ^{39}Mg, respectively. The calculation may be in contradiction with the observation for ^{35}Mg, where $J^\pi = 3/2^-$, a head of the $K^\pi = 1/2^-$ band, is suggested for the ground state [53]. We found that the binding energy obtained by blocking the $\Omega^\pi = 1/2^-$ orbital is shallower by 1.0 MeV. For ^{37}Mg, the measurements suggest that the $\ell = 1$ component is dominant in the ground state [5,6], while the $\Omega^\pi = 5/2^-$ orbital contains angular momenta higher than $\ell = 3$. Below, we discuss ^{37}Mg on this point. It is noted here that neutron superfluidity vanishes in ^{35,37}Mg.

Figure 2 shows the calculated one-neutron separation energies S_{n} compared with the experimental or evaluated data obtained from AME2016. Here, S_n is calculated as

$$S_n := -\left[B(N,Z) - B(N-1,Z)\right], \tag{79}$$

where $B(N,Z)$ is the (negative) binding energy of the nucleus with N neutrons and Z protons. A nice agreement within the error range and the odd–even staggering feature in the binding energies can be seen. It is noted that we need the binding energy of ^{33}Mg for the calculation of S_{n} of ^{34}Mg. We obtained the near degeneracy by blocking the $1/2^-$ and $7/2^-$ orbitals for ^{33}Mg. For ^{39}Mg, the calculated one-neutron separation energy is $S_n = -0.10$ MeV, the calculated chemical potential is

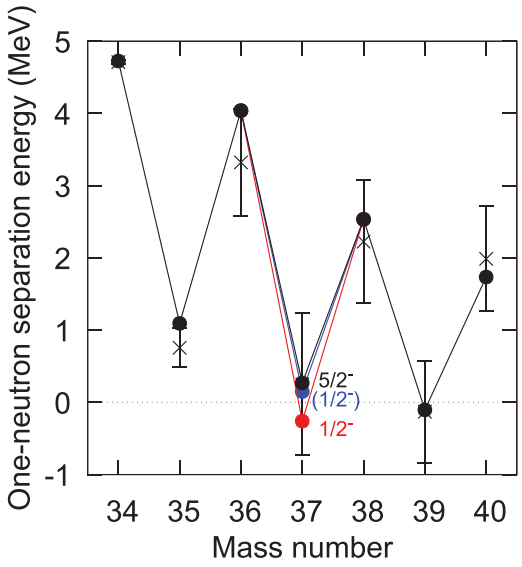

Fig. 2. Calculated one-neutron separation energies S_n of Mg isotopes denoted by closed circles together with the experimental data from AME2016 [46] denoted by crosses with error bars. For ^{37}Mg, the results obtained by blocking the $\Omega^\pi = 1/2^-$ orbital are also shown. The symbols for $(1/2^-)$ indicate the results obtained by ignoring the time-odd mean fields.

$\lambda^{\rm n} = -0.98$ MeV, and the qp energy of the blocked orbital is 0.83 MeV. Thus, the ^{39}Mg nucleus is unstable with respect to neutron emission, but bound, though quite loosely, in the sense that the sp energy of the last occupied neutron is negative in the present calculation. On the other hand, we could not find the bound-state solutions for ^{41,42}Mg.

We show with closed circles in Fig. 3 the calculated quadrupole-deformation parameters β_2 and matter radii $\sqrt{\langle r^2\rangle_{\rm m}}$, which are defined by

$$\beta_2 := \frac{4\pi}{5A\langle r^2\rangle_{\rm m}} \int d\boldsymbol{r} r^2 Y_{20}(\hat{r})\rho_0(\boldsymbol{r}), \tag{80}$$

$$\sqrt{\langle r^2\rangle_{\rm m}} := \sqrt{\frac{1}{A}\int d\boldsymbol{r} r^2 \rho_0(\boldsymbol{r})}. \tag{81}$$

As shown in Fig. 3(a), the Mg isotopes under study are calculated to be constantly deformed and this is consistent with the preceding theoretical predictions on the Mg isotopes near the drip line [49,54–60]. The odd–even staggering in deformation is faint compared with that of the one-neutron separation energies. Therefore, the odd–even staggering seen in the binding energy of these isotopes can be attributed mainly to the pair correlation.

Let us discuss the systematic feature in matter radii. Figure 3(b) shows the calculated matter radii $\sqrt{\langle r^2\rangle_{\rm m}}$ compared with the observation based on the reaction cross section measurement [61]. Except for ^{37}Mg, the present calculation reproduces the isotopic dependence observed experimentally. However, we see a systematic underestimation. This is mainly because the calculation gives a systematic over binding. The irregular dependence revealed in $^{34–36}$Mg by the reaction cross section measurement [5] is well described; the matter radius of ^{35}Mg is smaller than the average of the radii of the neighboring isotopes of ^{34,36}Mg. The suppression of the matter radius in ^{35}Mg can be attributed to the smaller deformation than in the neighboring isotopes, as shown in Fig. 3(a). To make this point clear, we shall adopt the following alternative expressions of the deformation and matter radius for

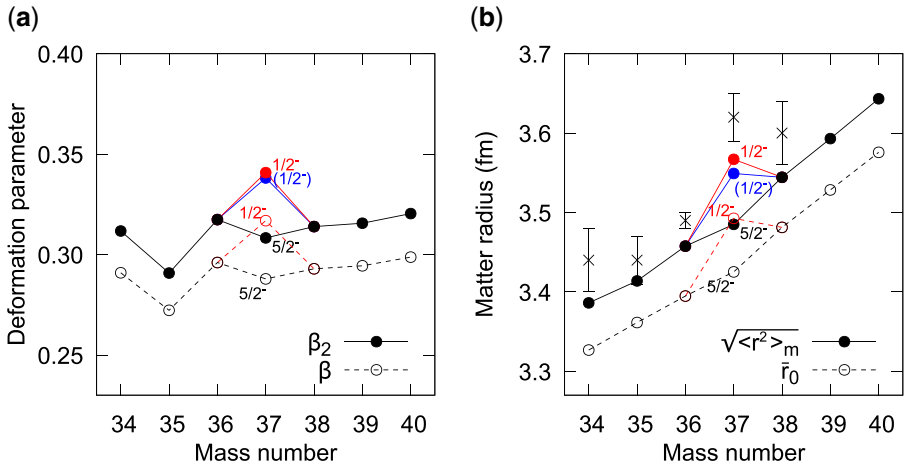

Fig. 3. (a) Calculated deformation parameters of Mg isotopes. The closed circles denote the quadrupole-deformation parameters β_2. For reference, the calculated β values defined in Eq. (82) are plotted by the open circles connected by the dashed line. (b) Matter radii of Mg isotopes. The closed circles denote the calculated matter radii $\sqrt{\langle r^2\rangle_m}$, compared with the observation denoted by the crosses with error bars taken from Ref. [61]. For reference, the calculated $\bar{r}_0$ values defined in Eq. (82) are plotted by the open circles connected by the dashed line. As in Fig. 2, the results obtained by blocking the $\Omega^\pi = 1/2^-$ orbital are also shown for ^{37}Mg. The symbols for $(1/2^-)$ indicate the results obtained by ignoring the time-odd mean fields.

axially symmetric nuclei [58,61]:

$$\langle x^2\rangle_{\rm m} = \langle y^2\rangle_{\rm m} = \frac{1}{A}\int d\boldsymbol{r}\frac{\varrho^2}{2}\rho_0(\boldsymbol{r}) =: \frac{\bar{r}_0^2}{3}\exp\left(-\sqrt{\frac{5}{4\pi}}\beta\right),$$
$$\langle z^2\rangle_{\rm m} = \frac{1}{A}\int d\boldsymbol{r} z^2\rho_0(\boldsymbol{r}) =: \frac{\bar{r}_0^2}{3}\exp\left(2\sqrt{\frac{5}{4\pi}}\beta\right). \tag{82}$$

One can see the relation as

$$\beta = \frac{1}{3}\sqrt{\frac{4\pi}{5}}\ln\left(\frac{1+2\sqrt{\frac{5}{4\pi}}\beta_2}{1-\sqrt{\frac{5}{4\pi}}\beta_2}\right) = \beta_2 - \frac{1}{4}\sqrt{\frac{5}{\pi}}\beta_2^2 + \mathcal{O}(\beta_2^3),$$
$$\bar{r}_0 = \sqrt{\langle r^2\rangle_{\rm m}}\left[\left(1-\sqrt{\frac{5}{4\pi}}\beta_2\right)^2\left(1+2\sqrt{\frac{5}{4\pi}}\beta_2\right)\right]^{\frac{1}{6}} = \sqrt{\langle r^2\rangle_{\rm m}}\left[1-\frac{5}{8\pi}\beta_2^2+\mathcal{O}(\beta_2^3)\right],$$

and $\beta \approx \beta_2$ and $\bar{r}_0 \approx \sqrt{\langle r^2\rangle_{\rm m}}$ for small deformation. The definitions of the deformation parameter β and radius $\bar{r}_0$ in Eq. (82) guarantee the volume conservation of a spheroidal nucleus whose density is given by $\rho_0 = A/V$ if $\varrho^2/a^2 + z^2/b^2 \le 1$ and zero if $\varrho^2/a^2 + z^2/b^2 > 1$, with $V = 4\pi a^2 b/3 = 4\pi/3(5\bar{r}_0/3)^{3/2}$ [62]. In terms of the parameters β and $\bar{r}_0$, the effects of the deformation and the spatial extension are decoupled in the spheroidal nuclei with a sharp surface owing to the volume conservation. We show the calculated β and $\bar{r}_0$ values in Fig. 3 with the open circles. The suppression of the matter radius $\sqrt{\langle r^2\rangle_{\rm m}}$ in ^{35}Mg disappears in $\bar{r}_0$, while the deformation is reduced in ^{35}Mg compared with ^{34,36}Mg in terms of β as well as β_2. This clearly shows that the reduction of the deformation accounts for the suppression of the matter radius in ^{35}Mg.

The discrepancy in the matter radius between calculation and observation for ^{37}Mg is due to the suppression of spatial extension caused by the high centrifugal barrier of the blocked orbital of $[312]5/2$ stemming from the $f_{7/2}$ shell. As mentioned above, the experimental measurements suggest that the ground state in ^{37}Mg is dominated by the p-wave [5,6]. When the deformation develops further, the $[312]5/2$ orbital crosses with the $[321]1/2$ orbital. The latter orbital is originating from the $p_{3/2}$ shell. Therefore, blocking the $\Omega^\pi = 1/2^-$ orbital is worth investigating. Indeed, the deformed halo structure in ^{37}Mg has been studied by assuming a high deformation of $\beta_2 \sim 0.5$ in a deformed Woods–Saxon potential to put a neutron in the $[321]1/2$ orbital on the even–even ^{36}Mg nucleus [63]. We show in Figs. 2 and 3 the results obtained by blocking the $\Omega^\pi = 1/2^-$ orbital for ^{37}Mg, as indicated by red circles. In Fig. 3(a), the matter radius increases by 0.08 fm by blocking the $\Omega^\pi = 1/2^-$ orbital. Then, we can see a sudden enhancement from ^{36}Mg. As expected, the deformation develops that we can see in Fig. 3(a). The matter quadrupole deformation obtained is $\beta_2 = 0.35$, and we see an increase in β_2 by 0.03, which is far lower than the phenomenological value [63]. Note that β and $\bar{r}_0$ contribute cooperatively to the enhancement of $\sqrt{\langle r^2\rangle_{\rm m}}$ in ^{37}Mg, indicating dilution of the density with deformation, in contrast to the case of ^{35}Mg, where only the deformation contributes to the suppression of the matter radius, as seen above and in Ref. [58]. The total binding energy calculated by blocking the $\Omega^\pi = 1/2^-$ orbital is shallower by 0.53 MeV, which we see in Fig. 2. We found that the neutrons in ^{37}Mg obtained by blocking the $\Omega^\pi = 1/2^-$ orbital are paired. The calculated chemical potential and the qp energy of the blocked orbital are -2.70 MeV and 2.20 MeV, respectively, while the sp energy of the last occupied neutron is -1.1 MeV obtained by blocking the $\Omega^\pi = 5/2^-$ orbital. The asymptotic behavior of the last occupied orbital is given as $r\varphi_{2,i}(\boldsymbol{r}) \sim \exp[-\sqrt{-2m(\lambda + E_i)}r/\hbar]$ for a paired system and $\sim \exp[-\sqrt{-2m\epsilon_i}r/\hbar]$ for an unpaired system, with ϵ_i being the sp energy [64]. Thus, we have enhancement in the radius by blocking the $\Omega^\pi = 1/2^-$ orbital, though the chemical potential is not very shallow. This can be considered as unpaired-particle haloing [58]. It should be noted that in Ref. [58] the self-consistent HFB calculation with a semirealistic interaction nicely produces the enhancement of the matter radius for the ground state in ^{37}Mg. Our framework is similar to that of Ref. [58]. The interactions used are different. This suggests that the ground-state property in ^{37}Mg can impose restrictions on the EDF.

To see the spatial structure of ^{37}Mg, we draw the calculated density distributions in terms of the equidensity lines on the ϱ–z plane in Fig. 4(a). The contour lines are depicted in a logarithmic scale at 0.1 fm^{-3} down to 10^{-7} fm^{-3}. In Fig. 4(b), the density distributions of neutrons along the symmetry axis (at $\varrho = 0.4$ fm) are also shown in a logarithmic scale. The density distributions obtained by blocking the $\Omega^\pi = 5/2^-$ and $1/2^-$ orbitals are presented. In the case of $\Omega^\pi = 5/2^-$, the density distribution of neutrons is well localized in the center, though the spatial extension is visible compared with that of protons, forming the neutron skin. Blocking the $\Omega^\pi = 1/2^-$ orbital drastically changes the distribution of neutrons. A long tail emerges, interpreted as the neutron halo. The spatial distribution is extended toward the symmetry axis, forming a peanut shape. This is consistent with the previous calculation [58], and results from the p-wave dominance near the continuum threshold [65–68].

The time-reversal symmetry is intrinsically broken in the odd-mass isotopes possessing nonzero spin, so that the time-odd components in the mean field may be activated. We discuss finally the roles of the time-odd mean fields in ^{37}Mg by blocking the $\Omega^\pi = 1/2^-$ orbital. The total binding energy is affected by 0.41 MeV, as shown in Fig. 2(a). Here, the time-odd fields are set to zero, i.e. equivalent to the equal-filling approximation. This is only 0.16% of the total binding energy, and is negligibly small. A tiny effect on the nuclear mass has been brought out by the systematic calculation

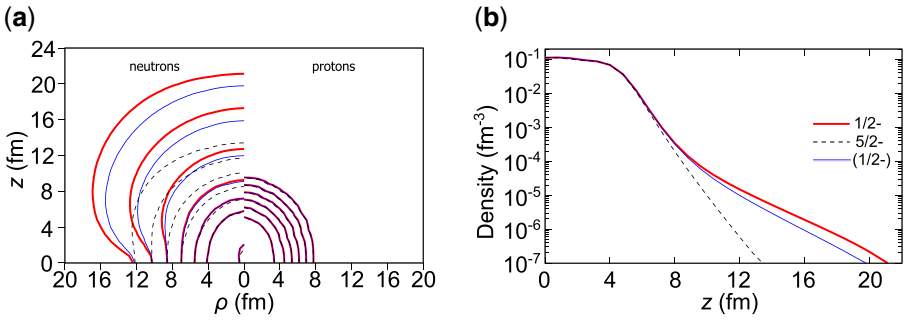

Fig. 4. (a) Contour plot of neutron and proton densities on the ϱ–z plane for ^{37}Mg. Positions of the density with 0.1, 0.01, 10^{-3}, 10^{-4}, 10^{-5}, 10^{-6}, and 10^{-7} fm^{-3} are presented. (b) Neutron density distributions along the symmetry axis. The results obtained by blocking the $\Omega^{\pi} = 1/2^{-}$ and $5/2^{-}$ orbitals are shown. In the case of $\Omega^{\pi} = 1/2^{-}$, also shown are the results obtained by ignoring the time-odd mean fields.

[12]. Accordingly, the deformation property is hardly influenced by the time-odd fields, as shown in Fig. 2(b). The deformation parameter for neutrons is reduced by 0.01. The radius of neutrons thus calculated is lessened by 0.02 fm, while the protons are not affected. Then, the matter radius is reduced by 0.02 fm, as shown in Fig. 3. The chemical potential and the qp energy of the blocked orbital are -2.73 MeV and 1.92 MeV, respectively. Then, the qp energy of the last neutron is lowered by 0.28 MeV by ignoring the time-odd fields. It seems that this shift is also negligible. However, the asymptotic behavior of the halo structure is sensitive to the exponent of the qp wave function. Indeed, as shown in Fig. 4, the tail structure is influenced by the time-odd fields. Whether the time-odd mean fields enhance or reduce the halo structure depends on the EDF employed. The spin-density term in the EDF, the first term on the right-hand side in Eq. (A.3), is responsible for the enhancement in the radius: the matter radius of ^{37}Mg obtained by ignoring all the time-odd fields except those derived from the spin-density term is no more than 0.02% different from the result obtained by including all the time-odd fields. The reaction observables sensitive to the outer surface of the halo nucleus can put constraints on the time-odd coupling constants, especially on the coefficient of the spin-density term, of the Skyrme EDF that are uncertain.

5. Summary

We have found relationships among the particle-number parity, the Bogoliubov transformation, and the time-reversal symmetry of the Hartree–Fock–Bogoliubov Hamiltonian. Then we showed that the lowest-energy solution of the HFB equation has even particle-number parity as long as the time-reversal symmetry is conserved in the HFB Hamiltonian without null eigenvalues. Based on this finding, we gave the foundation of a method for solving the HFB equation to describe the ground state of odd-mass nuclei by employing an appropriate time-reversal antisymmetric constraint operator to the Hamiltonian. With this procedure, one can directly obtain the ground state of an odd-mass nucleus as a self-consistent solution of the cranked-HFB-type equation, while the ground state of an odd-mass nucleus is described as a one-quasiparticle excitation of a neighboring even–even nucleus in the usual procedure. This method is further applicable to the low-lying two-quasiparticle excitations in even–even nuclei. As a numerical example, we applied this method to the neutron-rich Mg isotopes close to the drip line, and showed that the anomalous increase in the matter radius of ^{37}Mg is well described when a neutron occupies the low-Ω orbital in the framework of the nuclear

energy-density functional method. We found that the time-odd mean fields have little influence on the total binding energy, but an appreciable impact on the asymptotic behavior of the halo structure.

Acknowledgments

The authors thank A. Afanasjev, M. Grasso, N. Itagaki, M. Matsuo, T. Nakatsukasa, and D. Vretenar for valuable discussions and comments. This work was supported by the Japan Society for the Promotion of Science (JSPS) KAKENHI (Grants Nos. JP19K03824 and JP19K03872), and the JSPS-NSFC Bilateral Program for Joint Research Project on "Nuclear mass and life for unraveling mysteries of the r-process." The numerical calculations were performed on a CRAY XC40 at the Yukawa Institute for Theoretical Physics, Kyoto University.

Appendix A. Mean-field potentials for axially symmetric nuclei

In this appendix we give the explicit expressions of the mean-field potentials obtained from the Skyrme EDF and the pairing EDF for axially symmetric nuclei.

Appendix A.1. Mean-field potentials in the Skyrme EDF for axially symmetric nuclei

The Skyrme EDF consists of the time-even and time-odd parts [69]:

$$\mathcal{E}_{\rm Sky} = \int d\boldsymbol{r} \sum_{t=0,1} \Big[\mathscr{H}_t^{\rm even}(\boldsymbol{r}) + \mathscr{H}_t^{\rm odd}(\boldsymbol{r}) \Big], \tag{A.1}$$

where

$$\mathscr{H}_t^{\rm even} = C_t^{\rho}[\rho_0]\rho_t^2 + C_t^{\triangle\rho}\rho_t \triangle \rho_t + C_t^{\tau}\rho_t\tau_t + C_t^{J}\overleftrightarrow{J}_t{}^2 + C_t^{\nabla J}\rho_t \boldsymbol{\nabla}\cdot\boldsymbol{J}_t, \tag{A.2}$$

$$\mathscr{H}_t^{\rm odd} = C_t^{s}[\rho_0]\boldsymbol{s}_t^2 + C_t^{\triangle s}\boldsymbol{s}_t \cdot \triangle \boldsymbol{s}_t + C_t^{T}\boldsymbol{s}_t \cdot \boldsymbol{T}_t + C_t^{j}\boldsymbol{j}_t^2 + C_t^{\nabla j}\boldsymbol{s}_t \cdot (\boldsymbol{\nabla}\times\boldsymbol{j}_t), \tag{A.3}$$

with $t = 0$ and 1 denoting isoscalar and isovector, respectively. Here, the definitions of the densities and currents are given in Ref. [69]. Then, the mean-field potentials are given by the functional derivatives as [69,70]

$$\Gamma_{{\rm Sky},t}^{\rm even}(\boldsymbol{r}) = -\boldsymbol{\nabla}\cdot M_t(\boldsymbol{r})\boldsymbol{\nabla} + U_t(\boldsymbol{r}) + \frac{1}{2i}\Big[\overleftrightarrow{\nabla\sigma}\,\overleftrightarrow{B}_t(\boldsymbol{r}) + \overleftrightarrow{B}_t(\boldsymbol{r})\overleftrightarrow{\nabla\sigma}\Big] + \delta_{0t}U_0'(\boldsymbol{r}), \tag{A.4}$$

$$\Gamma_{{\rm Sky},t}^{\rm odd}(\boldsymbol{r}) = -\boldsymbol{\nabla}\cdot(\boldsymbol{\sigma}\cdot\boldsymbol{C}_t(\boldsymbol{r}))\boldsymbol{\nabla} + \boldsymbol{\sigma}\cdot\boldsymbol{\Sigma}_t(\boldsymbol{r}) + \frac{1}{2i}[\boldsymbol{\nabla}\cdot\boldsymbol{I}_t(\boldsymbol{r}) + \boldsymbol{I}_t(\boldsymbol{r})\cdot\boldsymbol{\nabla}]. \tag{A.5}$$

Here we used the symbol $\overleftrightarrow{\nabla\sigma} \coloneqq \boldsymbol{\nabla}\otimes\boldsymbol{\sigma}$, and

$$U_t = 2C_t^{\rho}\rho_t + 2C_t^{\triangle\rho}\triangle\rho_t + C_t^{\tau}\tau_t + C_t^{\nabla J}\boldsymbol{\nabla}\cdot\boldsymbol{J}_t, \tag{A.6}$$

$$\boldsymbol{\Sigma}_t = 2C_t^{s}\boldsymbol{s}_t + 2C^{\triangle s}\triangle\boldsymbol{s}_t + C_t^{T}\boldsymbol{T}_t + C_t^{\nabla j}\boldsymbol{\nabla}\times\boldsymbol{j}_t, \tag{A.7}$$

$$M_t = C_t^{\tau}\rho_t, \tag{A.8}$$

$$\boldsymbol{C}_t = C_t^{T}\boldsymbol{s}_t, \tag{A.9}$$

$$\overleftrightarrow{B}_t = 2C_t^{J}\overleftrightarrow{J}_t - C^{\nabla J}\overleftrightarrow{\nabla}\rho_t, \tag{A.10}$$

$$\boldsymbol{I}_t = 2C_t^{j}\boldsymbol{j}_t + C^{\nabla j}\boldsymbol{\nabla}\times\boldsymbol{s}_t, \tag{A.11}$$

$$U_0' = \sum_{t=0,1}\left(\frac{\partial C_t^{\rho}}{\partial\rho_0}\rho_t^2 + \frac{\partial C_t^{s}}{\partial\rho_0}\boldsymbol{s}_t^2\right), \tag{A.12}$$

where $\nabla_{\mu\nu} \coloneqq \sum_\kappa \epsilon_{\mu\nu\kappa}\nabla_\kappa$.

The mean-field potentials $\Gamma_{\rm Sky}$ are composed of the densities and currents, so we show the expressions in the cylindrical coordinates $\boldsymbol{r} = (\varrho, \phi, z)$ employing the ansätze in Eq. (73). The time-even densities are given as

$$\rho^q = \sum_i \left[(\varphi_{2,i}^{q+})^2 + (\varphi_{2,i}^{q-})^2 \right], \tag{A.13}$$

$$\begin{cases} J^q_{\varrho\phi} = -\sum_i (\varphi_{2,i}^{q+}\partial_\varrho \varphi_{2,i}^{q-} - \varphi_{2,i}^{q-}\partial_\varrho \varphi_{2,i}^{q+}), \\ J^q_{\phi\varrho} = \sum_i \dfrac{\Lambda_i^+ + \Lambda_i^-}{\varrho} \varphi_{2,i}^{q+}\varphi_{2,i}^{q-}, \\ J^q_{\phi z} = \sum_i \left[\dfrac{\Lambda_i^-}{\varrho}(\varphi_{2,i}^{q+})^2 - \dfrac{\Lambda_i^+}{\varrho}(\varphi_{2,i}^{q-})^2 \right], \\ J^q_{z\phi} = -\sum_i (\varphi_{2,i}^{q+}\partial_z \varphi_{2,i}^{q-} - \varphi_{2,i}^{q-}\partial_z \varphi_{2,i}^{q+}), \\ J^q_{\varrho\varrho} = J^q_{\phi\phi} = J^q_{zz} = J^q_{\varrho z} = J^q_{z\varrho} = 0, \end{cases} \tag{A.14}$$

and

$$\tau^q = \sum_i \left[(\partial_\varrho \varphi_{2,i}^{q+})^2 + (\partial_\varrho \varphi_{2,i}^{q-})^2 + \left(\frac{\Lambda_i^-}{\varrho}\varphi_{2,i}^{q+} \right)^2 + \left(\frac{\Lambda_i^+}{\varrho}\varphi_{2,i}^{q-} \right)^2 + (\partial_z \varphi_{2,i}^{q+})^2 + (\partial_z \varphi_{2,i}^{q-})^2 \right]. \tag{A.15}$$

The time-odd densities are

$$\begin{cases} s^q_\varrho = -2\sum_i \varphi_{2,i}^{q+}\varphi_{2,i}^{q-}, \\ s^q_z = -\sum_i \left[(\varphi_{2,i}^{q+})^2 - (\varphi_{2,i}^{q-})^2 \right], \\ s^q_\phi = 0, \end{cases} \tag{A.16}$$

$$\begin{cases} j^q_\phi = -\sum_i \left[\dfrac{\Lambda_i^-}{\varrho}(\varphi_{2,i}^{q+})^2 + \dfrac{\Lambda_i^+}{\varrho}(\varphi_{2,i}^{q-})^2 \right], \\ j^q_\varrho = j^q_\phi = 0, \end{cases} \tag{A.17}$$

and

$$\begin{cases} T^q_\varrho = -2\sum_i \left[(\partial_\varrho \varphi_{2,i}^{q+})(\partial_\varrho \varphi_{2,i}^{q-}) + (\partial_z \varphi_{2,i}^{q+})(\partial_z \varphi_{2,i}^{q-}) + \dfrac{\Lambda_i^-\Lambda_i^+}{\varrho^2}\varphi_{2,i}^{q+}\varphi_{2,i}^{q-} \right], \\ T^q_z = -\sum_i \left[(\partial_\varrho \varphi_{2,i}^{q+})^2 - (\partial_\varrho \varphi_{2,i}^{q-})^2 + \left(\dfrac{\Lambda_i^-}{\varrho}\varphi_{2,i}^{q+} \right)^2 - \left(\dfrac{\Lambda_i^+}{\varrho}\varphi_{2,i}^{q-} \right)^2 + (\partial_z \varphi_{2,i}^{q+})^2 - (\partial_z \varphi_{2,i}^{q-})^2 \right], \\ T^q_\phi = 0. \end{cases} \tag{A.18}$$

Substituting these densities into Eqs. (A.4) and (A.5), one obtains

$$\Gamma^{\rm even}_{{\rm Sky},t}(\boldsymbol{r}) = \begin{bmatrix} \Gamma^{\rm even}_{{\rm Sky},t\uparrow\uparrow}(\varrho,z;l_z) & e^{-i\phi}\Gamma^{\rm even}_{{\rm Sky},t\uparrow\downarrow}(\varrho,z;l_z) \\ e^{i\phi}\Gamma^{\rm even}_{{\rm Sky},t\downarrow\uparrow}(\varrho,z;l_z) & \Gamma^{\rm even}_{{\rm Sky},t\downarrow\downarrow}(\varrho,z;l_z) \end{bmatrix}, \tag{A.19}$$

$$\Gamma^{\rm odd}_{{\rm Sky},t}(\boldsymbol{r}) = \begin{bmatrix} \Gamma^{\rm odd}_{{\rm Sky},t\uparrow\uparrow}(\varrho,z;l_z) & e^{-i\phi}\Gamma^{\rm odd}_{{\rm Sky},t\uparrow\downarrow}(\varrho,z;l_z) \\ e^{i\phi}\Gamma^{\rm odd}_{{\rm Sky},t\downarrow\uparrow}(\varrho,z;l_z) & \Gamma^{\rm odd}_{{\rm Sky},t\downarrow\downarrow}(\varrho,z;l_z) \end{bmatrix}, \tag{A.20}$$

where

$$\Gamma^{\rm even}_{{\rm Sky},t\uparrow\uparrow} = -(\partial_\varrho M_t)\partial_\varrho - (\partial_z M_t)\partial_z - M_t\triangle + U_t + \delta_{0t}U'_0 + B_{t\phi z}\frac{l_z}{\varrho}, \tag{A.21}$$

$$\Gamma^{\rm even}_{{\rm Sky},t\uparrow\downarrow} = -K_t - B_{t\varrho\phi}\partial_\varrho - B_{tz\phi}\partial_z + B_{t\phi\varrho}\frac{l_z}{\varrho}, \tag{A.22}$$

$$\Gamma^{\rm even}_{{\rm Sky},t\downarrow\uparrow} = K_t + B_{t\varrho\phi}\partial_\varrho + B_{tz\phi}\partial_z + B_{t\phi\varrho}\frac{l_z}{\varrho}, \tag{A.23}$$

$$\Gamma^{\rm even}_{{\rm Sky},t\downarrow\downarrow} = -(\partial_\varrho M_t)\partial_\varrho - (\partial_z M_t)\partial_z - M_t\triangle + U_t + \delta_{0t}U'_0 - B_{t\phi z}\frac{l_z}{\varrho}, \tag{A.24}$$

$$\Gamma^{\rm odd}_{{\rm Sky},t\uparrow\uparrow} = -(\partial_\varrho C_{tz})\partial_\varrho - (\partial_z C_{tz})\partial_z - C_{tz}\triangle + \Sigma_{tz} + I_{t\phi}\frac{l_z}{\varrho}, \tag{A.25}$$

$$\Gamma^{\rm odd}_{{\rm Sky},t\uparrow\downarrow} = -(\partial_\varrho C_{t\varrho})\partial_\varrho - (\partial_z C_{t\varrho})\partial_z - C_{t\varrho}\triangle + \Sigma_{t\varrho} - C_{t\varrho}\frac{l_z}{\varrho^2}, \tag{A.26}$$

$$\Gamma^{\rm odd}_{{\rm Sky},t\downarrow\uparrow} = -(\partial_\varrho C_{t\varrho})\partial_\varrho - (\partial_z C_{t\varrho})\partial_z - C_{t\varrho}\triangle + \Sigma_{t\varrho} + C_{t\varrho}\frac{l_z}{\varrho^2}, \tag{A.27}$$

$$\Gamma^{\rm odd}_{{\rm Sky},t\downarrow\downarrow} = (\partial_\varrho C_{tz})\partial_\varrho + (\partial_z C_{tz})\partial_z + C_{tz}\triangle - \Sigma_{tz} + I_{t\phi}\frac{l_z}{\varrho}. \tag{A.28}$$

Here, $l_z = \frac{\partial_\phi}{i}$ and we defined

$$\begin{aligned} K_t &\coloneqq \frac{1}{2}\left[(\partial_\varrho B_{t\varrho\phi}) + (\partial_z B_{tz\phi}) + \frac{1}{\varrho}(B_{t\varrho\phi} + B_{t\phi\varrho})\right] \\ &= C^J_t\left[(\partial_\varrho J_{t\varrho\phi}) + (\partial_z J_{tz\phi}) + \frac{1}{\varrho}(J_{t\varrho\phi} + J_{t\phi\varrho})\right]. \end{aligned} \tag{A.29}$$

Appendix A.2. Mean-field potentials in the pairing EDF for axially symmetric nuclei

For the pairing energy, we adopt the following density functional:

$$\mathcal{E}_{\rm pair} = \frac{V_0}{4}\int d\boldsymbol{r}\left\{1 - V_1\left[\frac{\rho_0(\boldsymbol{r})}{\rho_{\rm c}}\right]^\gamma\right\}\sum_{q={\rm p,n}}|\tilde{\rho}^q(\boldsymbol{r})|^2, \tag{A.30}$$

where $\tilde{\rho}^q$ is the pairing density [64] and $\rho_{\rm c}$ is the saturation density. The contributions to the particle–hole potentials are given by

$$\Gamma^{\rm even}_{{\rm pair},t\,\sigma\sigma'}(\boldsymbol{r}) = \delta_{0t}\delta_{\sigma\sigma'}U_{\rm pair}(\boldsymbol{r}), \qquad \Gamma^{\rm odd}_{{\rm pair},t\,\sigma\sigma'}(\boldsymbol{r}) = 0, \tag{A.31}$$

where

$$U_{\rm pair} = -\frac{\gamma V_0 V_1}{4\rho_{\rm c}}\left(\frac{\rho_0}{\rho_{\rm c}}\right)^{\gamma-1}\sum_{q={\rm p,n}}|\tilde{\rho}^q|^2, \tag{A.32}$$

and the particle–particle potential, or the pair Hamiltonian, is given by

$$\tilde{h}^q_{\sigma\sigma'}(\boldsymbol{r}) = \delta_{\sigma\sigma'}\tilde{U}^q(\boldsymbol{r}), \tag{A.33}$$

where

$$\tilde{U}^q = \frac{V_0}{2}\left[1 - V_1\left(\frac{\rho_0}{\rho_c}\right)^\gamma\right]\tilde{\rho}^q. \tag{A.34}$$

With the axial symmetry, the pairing density in the cylindrical coordinates $\boldsymbol{r} = (\varrho, \phi, z)$ is given by employing the ansätze in Eq. (73) as

$$\tilde{\rho}^q = -\sum_i \left[\varphi^{q+}_{2,i}\varphi^{q+}_{1,i} + \varphi^{q-}_{2,i}\varphi^{q-}_{1,i}\right]. \tag{A.35}$$

In the end, one obtains

$$\Gamma^{\text{even}}_{\text{pair},t}(\boldsymbol{r}) = \delta_{0t}\begin{bmatrix} U_{\text{pair}}(\varrho, z) & 0 \\ 0 & U_{\text{pair}}(\varrho, z)\end{bmatrix}, \qquad \Gamma^{\text{odd}}_{\text{pair},t}(\boldsymbol{r}) = 0, \tag{A.36}$$

and

$$\tilde{h}^q(\boldsymbol{r}) = \begin{bmatrix} \tilde{U}^q(\varrho, z) & 0 \\ 0 & \tilde{U}^q(\varrho, z)\end{bmatrix}. \tag{A.37}$$

References

[1] T. Nakamura, H. Sakurai, and H. Watanabe, Prog. Part. Nucl. Phys. **97**, 53 (2017).
[2] B. A. Marsh et al., Nature Phys. **14**, 1163 (2018).
[3] T. Nakamura et al., Phys. Rev. Lett. **103**, 262501 (2009).
[4] M. Takechi et al., Phys. Lett. B **707**, 357 (2012).
[5] M. Takechi et al., Phys. Rev. C **90**, 061305(R) (2014).
[6] N. Kobayashi et al., Phys. Rev. Lett. **112**, 242501 (2014).
[7] M. Bender, P.-H. Heenen, and P.-G. Reinhard, Rev. Mod. Phys. **75**, 121 (2003).
[8] T. Nakatsukasa, K. Matsuyanagi, M. Matsuo, and K. Yabana, Rev. Mod. Phys. **88**, 045004 (2016).
[9] J. Erler, N. Birge, M. Kortelainen, W. Nazarewicz, E. Olsen, A. M. Perhac, and M. Stoitsov, Nature **486**, 509 (2012).
[10] A. V. Afanasjev, S. E. Agbemava, D. Ray, and P. Ring, Phys. Lett. B **726**, 680 (2013).
[11] P. Ring and P. Schuck, *The Nuclear Many-Body Problem* (Springer, New York, 1980).
[12] N. Schunck, J. Dobaczewski, J. McDonnell, J. Moré, W. Nazarewicz, J. Sarich, and M. V. Stoitsov, Phys. Rev. C **81**, 024316 (2010).
[13] M. V. Stoitsov, J. Dobaczewski, W. Nazarewicz, S. Pittel, and D. J. Dean, Phys. Rev. C **68**, 054312 (2003).
[14] G. F. Bertsch, C. A. Bertulani, W. Nazarewicz, N. Schunck, and M. V. Stoitsov, Phys. Rev. C **79**, 034306 (2009).
[15] L. S. Kisslinger and R. A. Sorensen, Rev. Mod. Phys. **35**, 853 (1963); **36**, 1104 (1964) [erratum].
[16] S. Perez-Martin and L. M. Robledo, Phys. Rev. C **78**, 014304 (2008).
[17] U. Hofmann and P. Ring, Phys. Lett. B **214**, 307 (1988).
[18] A. V. Afanasjev and P. Ring, Phys. Rev. C **62**, 031302(R) (2000).
[19] A. V. Afanasjev and H. Abusara, Phys. Rev. C **81**, 014309 (2010).
[20] A. V. Afanasjev and S. Shawaqfeh, Phys. Lett. B **706**, 177 (2011).
[21] K. Sugawara, Prog. Theor. Phys. **35**, 44 (1966).
[22] P.-H. Heenen, P. Bonche, and H. Flocard, Nucl. Phys. A **588**, 490 (1995).
[23] T. Duguet, P. Bonche, P.-H. Heenen, and J. Meyer, Phys. Rev. C **65**, 014310 (2001).

[24] G. Bertsch, J. Dobaczewski, W. Nazarewicz, and J. Pei, Phys. Rev. A **79**, 043602 (2009).
[25] H. Kasuya and K. Yoshida, JPS Conf. Proc. **31**, 011067 (2020).
[26] B. Banerjee, P. Ring, and H. J. Mang, Nucl. Phys. A **221**, 564 (1974).
[27] C. Bloch and A. Messiah, Nucl. Phys. **39**, 95 (1962).
[28] A. K. Kerman, Ann. Phys. **12**, 300 (1961).
[29] B. Banerjee, H. J. Mang, and P. Ring, Nucl. Phys. A **215**, 366 (1973).
[30] H. E. Haber, *Notes on antisymmetric matrices and the pfaffian* (University of California, Santa Cruz, 2015) (available at: http://scipp.ucsc.edu/ haber/webpage/pfaffian2.pdf, date last accessed August 8, 2020).
[31] L. M. Robledo, Phys. Rev. C **79**, 021302(R) (2009).
[32] A. Yu. Kitaev, Phys.-Usp. **44**, 131 (2001).
[33] A. L. Goodman, Nucl. Phys. A **230**, 466 (1974).
[34] P. Ring, H. J. Mang, and B. Banerjee, Nucl. Phys. A **225**, 141 (1974).
[35] M. Matsuo, Nucl. Phys. A **696**, 371 (2001).
[36] J. Dobaczewski and P. Olbratowski, Comp, Phys. Commun. **158**, 158 (2004).
[37] D. Vautherin, Phys. Rev. C **7**, 296 (1973).
[38] E. Terán, V. E. Oberacker, and A. S. Umar, Phys. Rev. C **67**, 064314 (2003).
[39] A. Blazkiewicz, V. E. Oberacker, A. S. Umar, and M. Stoitsov, Phys. Rev. C **71**, 054321 (2005).
[40] K. Yoshida and N. Van Giai, Phys. Rev. C **78**, 014305 (2008).
[41] H. Oba and M. Matsuo, Prog. Theor. Phys. **120**, 143 (2008).
[42] J. C. Pei, M. V. Stoitsov, G. I. Fann, W. Nazarewicz, N. Schunck, and F. R. Xu, Phys. Rev. C **78**, 064306 (2008).
[43] E. Anderson et al., *LAPACK Users' Guide*, (Society for Industrial and Applied Mathematics, Philadelphia, PA, 1999), 3rd ed.
[44] A. Baran, A. Bulgac, M. McNeil Forbes, G. Hagen, W. Nazarewicz, N. Schunck, and M. V. Stoitsov, Phys. Rev. C **78**, 014318 (2008).
[45] E. Chabanat, P. Bonche, P. Haensel, J. Meyer, and R. Schaeffer, Nucl. Phys. A **635**, 231 (1998).
[46] M. Wang, G. Audi, F. G. Kondev, W. J. Huang, S. Naimi, and X. Xu, Chin. Phys. C **41**, 030003 (2017).
[47] W. Satuła, J. Dobaczewski, and W. Nazarewicz, Phys. Rev. Lett. **81**, 3599 (1998).
[48] M. Kimura and H. Horiuchi, Prog. Theor. Phys. **107**, 33 (2002).
[49] R. Rodríguez-Guzmán, J. L. Egido, and L. M. Robledo, Nucl. Phys. A **709**, 201 (2002).
[50] N. Hinohara, K. Sato, K. Yoshida, T. Nakatsukasa, M. Matsuo, and K. Matsuyanagi, Phys. Rev. C **84**, 061302(R) (2011).
[51] M. Kimura, Int. J. Mod. Phys. E **20**, 893 (2011).
[52] M. Kimura, arXiv:1105.3281 [nucl-th] [Search INSPIRE].
[53] S. Momiyama et al., Phys. Rev. C, **96**, 034328 (2017).
[54] J. Terasaki, H. Flocard, P.-H. Heenen, and P. Bonche, Nucl. Phys. A **621**, 706 (1997).
[55] K. Yoshida, Eur. Phys. J. A **42**, 583 (2009).
[56] L. Li, J. Meng, P. Ring, E.-G. Zhao, and S.-G. Zhou, Phys. Rev. C **85**, 024312 (2012).
[57] M. Shimada, S. Watanabe, S. Tagami, T. Matsumoto, Y. R. Shimizu, and M. Yahiro, Phys. Rev. C **93**, 064314 (2016).
[58] H. Nakada and K. Takayama, Phys. Rev. C **98**, 011301(R) (2018).
[59] F. Nowacki and A. Poves, Phys. Rev. C **79**, 014310 (2009).
[60] E. Caurier, F. Nowacki, and A. Poves, Phys. Rev. C **90**, 014302 (2014).
[61] S. Watanabe et al., Phys. Rev. C **89**, 044610 (2014).
[62] D. L. Hill and J. A. Wheeler, Phys. Rev. **89**, 1102 (1953).
[63] Y. Urata, K. Hagino, and H. Sagawa, Phys. Rev. C **96**, 064311 (2017).
[64] J. Dobaczewski, H. Flocard, and J. Treiner, Nucl. Phys. A **422**, 103 (1984).
[65] T. Misu, W. Nazarewicz, and S. Åberg, Nucl. Phys. A **614**, 44 (1997).
[66] I. Hamamoto, Phys. Rev. C **69**, 041306(R) (2004).
[67] K. Yoshida and K. Hagino, Phys. Rev. C **72**, 064311 (2005).
[68] S.-G. Zhou, J. Meng, P. Ring, and E.-G. Zhao, Phys. Rev. C **82**, 011301(R) (2010).
[69] Y. M. Engel, D. M. Brink, K. Goeke, S. J. Krieger, and D. Vautherin, Nucl. Phys. A **249**, 215 (1975).
[70] J. Dobaczewski and J. Dudek, Phys. Rev. C **52**, 1827 (1995); **55**, 3177 (1997) [erratum].